On the Nature of Lone Pair–Surface Bonds and Their Scaling Relations

Arvin Kakekhani,[†] Luke T. Roling,[†] Ambarish Kulkarni,[†] Allegra A. Latimer,[†] Hadi Abroshan,[†] Julia Schumann,[†] Hassan AlJama,[†] Samira Siahrostami,[†] Sohrab Ismail-Beigi,[‡] Frank Abild-Pedersen,[†,¶] and Jens K. Nørskov[*,†,¶]

†*SUNCAT Center for Interface Science and Catalysis, Department of Chemical Engineering, Stanford University, Stanford, CA 94305, United States*

‡*Department of Applied Physics, Yale University, New Haven, CT 06520, United States*

¶*SUNCAT Center for Interface Science and Catalysis, SLAC National Accelerator Laboratory, Menlo Park, CA 94025, United States*

E-mail: norskov@stanford.edu

Abstract

We investigate the (surface) bonding of a class of industrially and biologically important molecules in which the chemically active orbital is a $2p$ electron lone-pair located on N or O atom bound via single bonds to H or alkyl groups. This class includes water, ammonia, alcohols, ethers and amines. Using extensive density functional theory (DFT) calculations, we discover scaling relations (correlations) among molecular binding energies of different members of this class: the bonding energetics of a single member can be used as a descriptor for other members. We investigate the bonding mechanism for a representative (H_2O), and find the most important physical surface properties that dictate the strength and nature of the bonding through a combination of covalent and non-covalent electrostatic effects. We describe the importance of surface

intrinsic electrostatic, geometric and mechanical properties in determining the extent of the lone pair–surface interactions. We study systems including ionic materials in which the surface positive and negative centers create strong local surface electric fields, which polarize the dangling lone-pair and lead to a strong "electrostatically-driven bond". We emphasize the importance of non-covalent electrostatic effects and discuss why a fully covalent picture, common in the current first-principles literature on surface bonding of these molecules, is not adequate to correctly describe the bonding mechanism and energy trends. By pointing out a completely different mechanism (charge transfer) as the major factor for binding N and O containing unsaturated (radical) adsorbates, we explain why their binding energies can be tuned independently from those of the aforementioned species, having potential implications in scaling-driven catalyst discovery.

Introduction

Scaling relations or linear correlations among binding energies (BEs) of adsorbates are at the heart of the computational catalyst design[1–3]. The many-dimensional search space for the optimum catalyst can be significantly reduced to a low-dimensional space of few descriptors due to such relations[4–8]. Most literature on scalings has focused on relations among open-shell unsaturated intermediates (eg., O*, OH*, OOH*). However a similar understanding of closed-shell adsorbates is lacking. Here, we show broadly applicable, material-independent scaling relations among a class of closed-shell molecules, whose chemically active orbital (HOMO) is an N- or O-2p lone-pair[9], in which the N or O is bound to neighboring atoms and groups in the molecule via single bonds. This class includes water, ammonia, alcohols, ethers and amines, which find use in medical, biological, pharmaceutical, fertilizer and fuel industries[10–13]. While there are studies that calculate BEs of these molecules[14–30] on specific surfaces, here we obtain a generalized understanding of their binding mechanisms and BE trends on a wide range of materials. The application of this descriptor-based approach[31–34] goes beyond merely predicting BEs, also implying the existence of a common

lone pair–surface bonding mechanism. We pick H_2O as a representative of the class, study its bonding and shed light on this common mechanism.

Our choice of H_2O stems from the essential role of water-surface interactions in a wide range of fields, from catalysis, electrocatalysis and surface wetting to corrosion of solids[35–39]. Water binding to transition metal (TM) surfaces has been extensively studied, especially in the context of water layer structures at the solid interface[40–43]. Here, we first introduce a simple electronic structure descriptor that models the water–TM interaction as a covalent interaction between the water HOMO and the surface empty bands. The interaction between water and clean TM surfaces[44] leads to a weak binding[45–47]. In contrast, on more ionic systems including oxides, several studies observe much stronger BEs[48]. This sizable span of BEs from a few tenths of an eV on TMs[44,49] to more than 1 eV on some oxide surfaces[48,50]combined with variations within the class of oxides[48] leads us to discover what dictates the strength of lone pair–surface interactions. By extending our covalent model for H_2O binding on clean TM surfaces to other surfaces, we disentangle the covalent and non-covalent contributions to the BEs. We show how non-covalent interactions become important and sometimes dominate when departing from bare TM surfaces. Non-covalent lone-pair interactions[51–62] have been discussed previously in the molecular chemistry literature, e.g., lone pair-π interactions[63–67]. We show that intrinsic surface electrostatics can polarize the dangling water HOMO and greatly stabilize its molecular bonding. The polarized lone-pair[68] then acts as an enhanced (induced) dipole that interacts with the local electrostatic potential well[69] created by the surface positive and negative centers. We explain the role of formal charges, geometry and surface electronic and mechanical properties on the BEs. Such knowledge can then be used to predict the water interaction with a wide range of surfaces, and has applications in electrocatalysis and electrochemistry[70–72], surface wetting[73–77], solid-water interfaces beyond TMs[78–85], solids corrosion[38,86,87], biological systems,[88,89] etc. As a consequence of the material-independent scaling relations we find between the N- and O-2p lone-pair species, such knowledge is transferrable to other molecules in this class.

Results and discussion

Material-independent lone-pair scaling relations

We conducted DFT calculations to study molecular (intact) lone-pair bonding on a large and diverse set of surfaces (a complete list in section 24 of the SI). Figure 1 (a) shows the H_2O and CH_3OH BEs scale broadly. We also investigated the scaling between O-2p and N-2p lone-pairs through H_2O and NH_3 (Fig. 1 (b)).

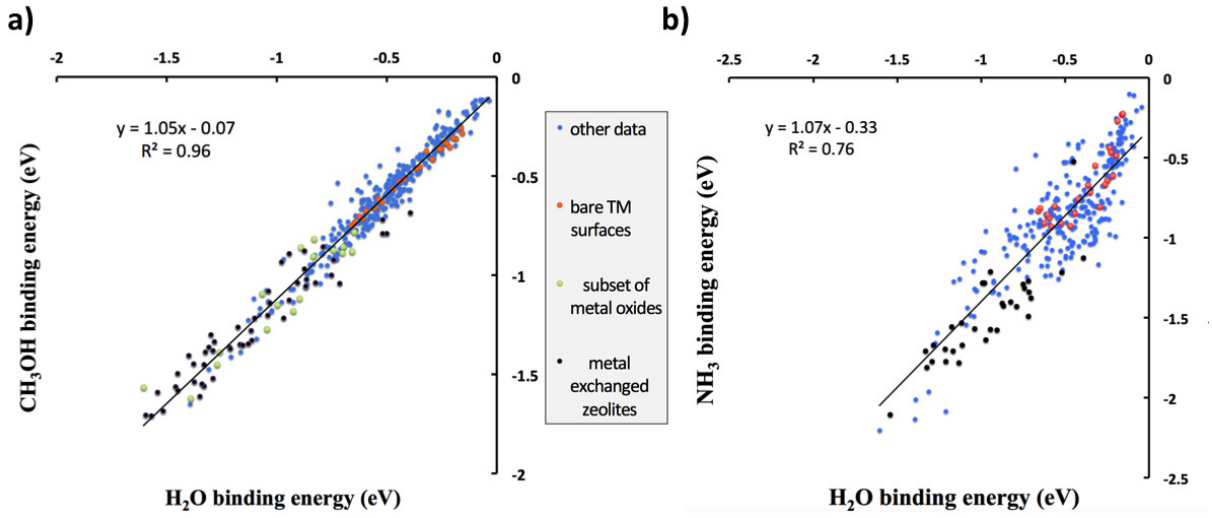

Figure 1: Scaling relations between BEs of (a) CH_3OH vs. H_2O and (b) NH_3 vs H_2O.

In order to understand these correlations, we plot the DFT-derived molecular orbitals (MOs) and their energies in Fig. 2. Details on the level alignments are in section 1 of the SI. The broadly observed scaling relations imply a similar surface bonding mechanism and therefore require similarities in the electronic structure[1,3]. Clearly, for these species, the character of the chemically active orbital (HOMO) is similar (O- or N-2p lone pair). Since we have already observed a correlation between BEs of H_2O, CH_3OH and NH_3, we expect that there should be similar relationships between all the considered molecules. In Fig. 3 we show the correlations based on BE calculations on a diverse subset of materials (see section 24.3 of the SI). The coefficients of determination are very high in all cases: we are able to predict the BE for any of these molecules by knowing only the BE of one of them.

Comparing Fig. 1(b) with the other plots in Figures 1 and 3, we notice a greater scatter when we compare species with O- versus N-2p. For example, the mean absolute error (MAE) is 0.05 eV in Fig. 1(a) and 0.15 eV in Fig. 1(b). Both MAEs are significantly smaller than the range of variations in BEs of the species across different materials (> 2 eV). Thus, the correlation in Fig. 1 (b) is meaningful and strong enough to indicate a common bonding mechanism across both the O and N-2p lone-pair species discussed here (an explicit comparison in section 20 of the SI).

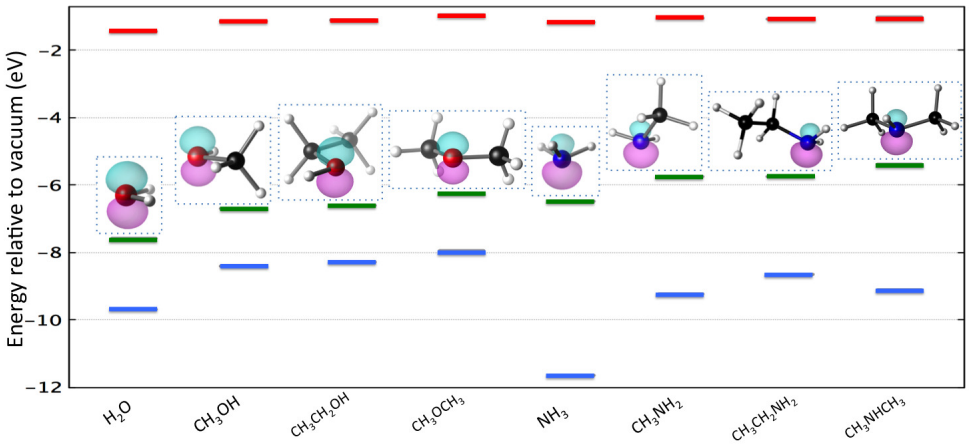

Figure 2: DFT-derived MOs for some molecular species with O- or N-2p lone pairs. The lines indicated in green show the HOMO, blue is HOMO-1 and red denotes LUMO. For the HOMO, we have graphically shown the MO by plotting the wavefunction: magenta and cyan show different signs of the wavefunction.

Lone pair–surface bond on clean transition metal surfaces

Due to the aforementioned scalings, we will focus primarily on the water-surface interaction as the class descriptor. Abild-Pedersen et. al.[1] have described scaling relations between BE of hydrogen containing adsorbates on TM surfaces. The BE of hydrogenated species AH_x is linked to that of the central atom A via:

$$E_{ads}(AH_x) = \gamma E_{ads}(A) + \xi \tag{1}$$

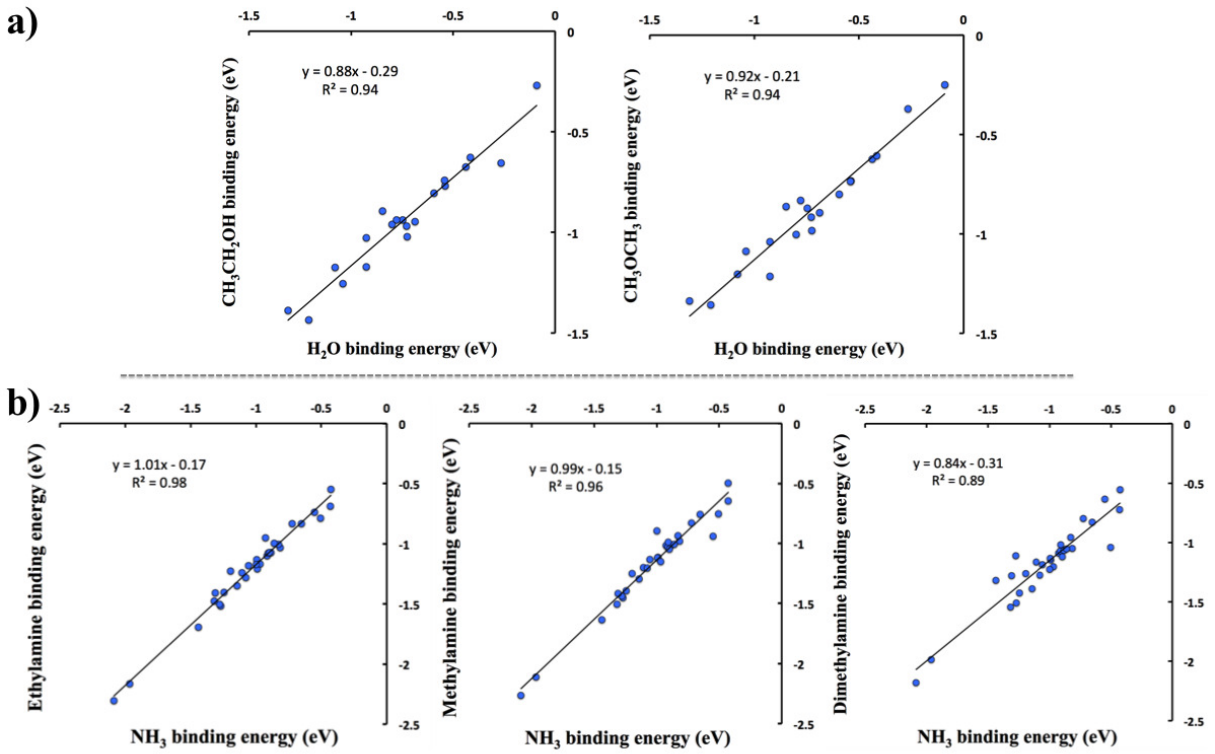

Figure 3: Scaling relations between (a) dimethyl ether, ethanol and water and (b) methylamine, ethylamine, dimethylamine and ammonia.

$$\gamma = \frac{(x_{max} - x)}{x_{max}} \tag{2}$$

where x_{max} is the maximum number of H atoms that can bond to A to form a stable gas-phase molecule (e.g., 2 for O and 3 for N). The largest contribution to the bonding of AH_x ($x < x_{max}$) species on TMs come from hybridization and charge transfer from the metal sp states[1,90]. This is approximately constant among TMs and the variation among different metals comes from a smaller contribution caused by the metal d states (ΔE_d)[1,90]. When $x = x_{max}$ e.g., $x = 4$ in CH_4, the H atoms bonded to the central atom provide it with the optimum charge density and according to eq. 2 the scaling parameter $\gamma = 0$.

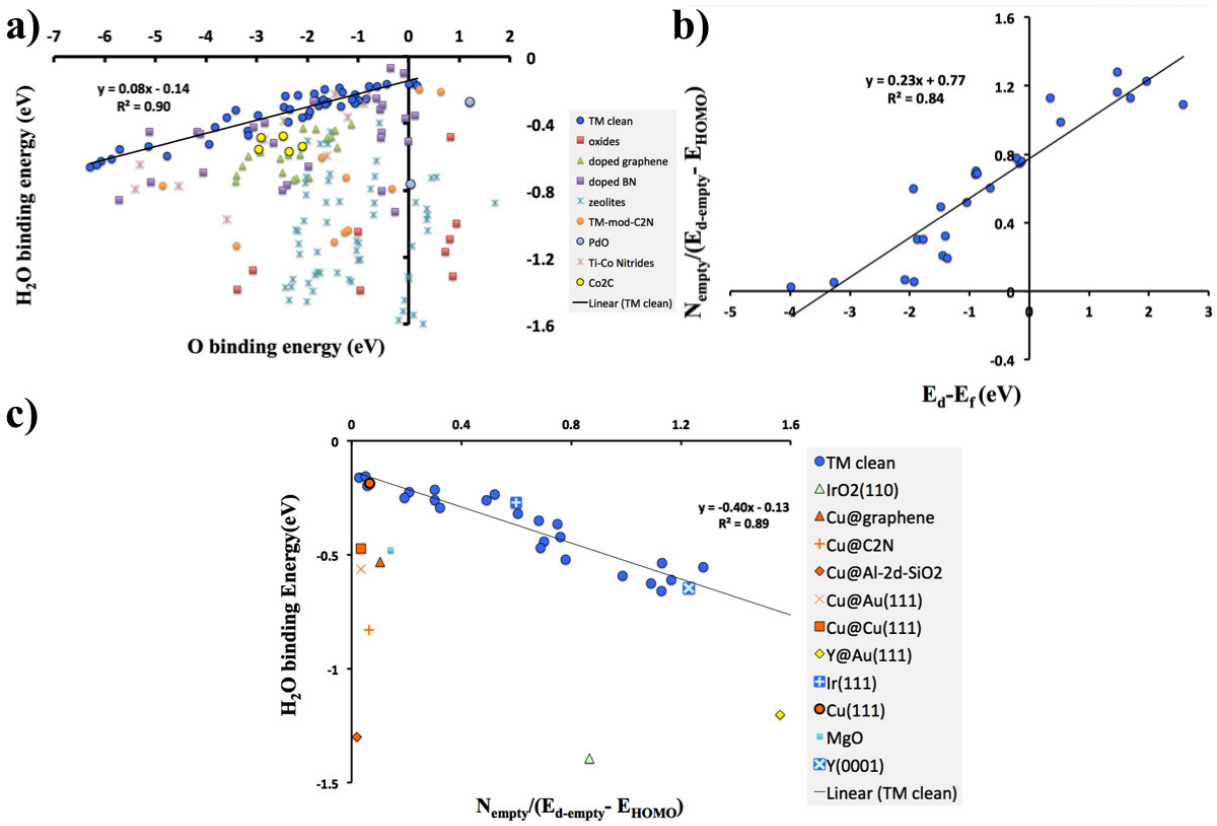

Figure 4: a) H_2O BE versus O on a number of TMs, oxides, nitrides, carbides and single site systems. b) The new descriptor $N_{empty}/(E_{d-empty}\text{- }E_{HOMO})$ scales with previously used descriptor for adsorbates' binding to TM surfaces E_d-E_f (center of d-band relative to Fermi energy). c) H_2O BE scales with $N_{empty}/(E_{d-empty}\text{- }E_{HOMO})$ for TM surfaces but not for other systems. O BE is relative to $\frac{1}{2}$ O_2, while H_2O binding is relative to H_2O in vacuum.

Here, we investigate the relation among H_2O and O BE for a diverse set of materials (Fig. 4(a)). For clean TM surfaces, the binding geometry is characterized by an almost flat on-top geometry (the normal to the H_2O plane being almost parallel to the surface normal and the oxygen on top of the surface metal), consistent with the literature[15,16,44,86,91–93]. On clean TM surfaces H_2O BE scales with O with a non-zero slope and y-intercept of $\gamma \approx 0.08$ and $\xi \approx -0.14$ eV. Below we describe the physics behind this non-zero γ.

The H_2O HOMO is a dangling filled O-2p state perpendicular to the H_2O plane (Fig. 2) denoted as a $1b_1$ MO[94–96]. Such a filled orbital can, in principle, interact with the unoccupied part of the surface conduction band and lower its energy[97–99]. Looking at projected density of states (PDOS) plots[100–102], this is manifested as an increased broadening of the adsorbed H_2O HOMO and an increased mixing between H_2O and metal states (Fig. 5). For details see section 2 of the SI.

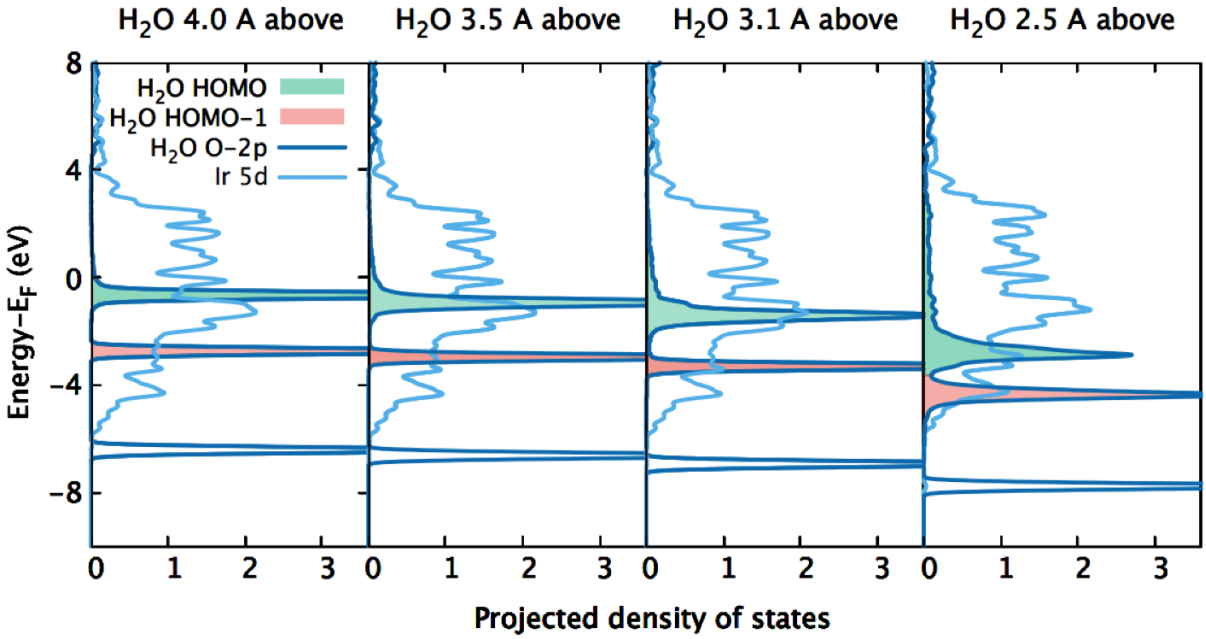

Figure 5: PDOS for H_2O adsorption on the Ir(111) surface.

Unlike the bond between AH_x ($x < x_{max}$) species and TM surfaces, dominated by electron transfer to the adsorbates states[1,90], the aforementioned bond is not associated with electron transfer from the surface to the closed-shell molecule. Some of the adsorbates with

$x = x_{max}$ like H_2O and NH_3 have dipole moments which can induce a dipole moment in the metal[103] (i.e., induced image charges in the metal[104]). The induced dipole further polarizes the molecule[19,103,105], and further stabilizes the lone-pair surface bond[44,45,104,106]. This interaction shows up in PDOS plots as a gradual energy downshift of the center of the H_2O HOMO as it approaches the surface (Fig. 5). There are also van der Waals (vdW) interactions that further stabilize the bonding[107–109]. Theoretical surveys find the magnitude of the vdW interaction to be $\lessapprox 0.2$ eV per H_2O molecule[107,110–112]. Despite the large number of factors that might affect the surface–water bonding, we find that a simple model in which the water HOMO interacts with the empty part of the d-band (above E_F) captures the variations in water BE among different TMs.

First, we turn to the Newns-Anderson (NA) model . As pointed out by Bligaard and Nørskov[113], in the limit of small surface-adsorbate coupling $|V_{ad}| \ll E_d - E_a$, the bond energy between a completely filled state $|a\rangle$ and a partially-filled state $|d\rangle$ (with filling f) is given by:

$$\delta E \propto \frac{(1-f)}{E_d - E_a} V_{ad}^2 \tag{3}$$

$$(1-f) \propto N_{empty} \tag{4}$$

Here N_{empty} is the total number of states above the Fermi energy for the surface chemically active $|d\rangle$ orbital. If we take the adsorbate filled state $|a\rangle$ to be the water HOMO then for a constant coupling constant V_{ad}:

$$\delta E \propto \frac{N_{empty}}{E_d - E_{HOMO}} \tag{5}$$

We find that for clean TM surfaces, the right hand side of eq. 5 correlates extremely well with a new descriptor in which E_d (center of the d-band) is substituted by $E_{d-empty}$ the center of the empty fraction of the d-band:

$$\frac{N_{empty}}{E_d - E_{HOMO}} \propto \frac{N_{empty}}{E_{d-empty} - E_{HOMO}} \tag{6}$$

The right hand side of eq. 6, to which we refer as Empty Band Descriptor (EBD) correlates with the center of the *d*-band which is the more frequently used descriptor[114–116] for radical adsorbates' (including O) interaction with TM surfaces (Fig. 4 (b)). We find that H_2O BEs on TM clean surfaces correlates with the EBD (Fig. 4 (c)) and consequently the center of the *d*-band. This is the underlying reason for the scaling between H_2O and O on clean TM surfaces (Fig. 4 (a)).

Choosing EBD as a descriptor means we model the H_2O molecular bonding as a chemical bond between the O-2*p* lone-pair (HOMO) and center of the empty part of surface *d*-band. This useful correlation between H_2O BE on clean TM surfaces and EBD is quantified by the simple relation:

$$E_{bind}(H_2O - TM_{clean}) = E_{bind}^{covalent}(H_2O) \approx -0.39\,(\text{eV})^2 \frac{N_{empty}}{E_{d-empty} - E_{HOMO}} - 0.13\,(\text{eV}) \tag{7}$$

Equation 7 can be extended beyond the simple case of transition metals (section 3 of the SI) to separate the covalent contribution to the lone pair–surface bonding from non-covalent contributions that will be discussed later in this article.

Table 1: H_2O and O BEs on a Cu atom in different host structures. The oxidation state (without adsorbates) is calculated using Bader charge analysis (BCA). O binding is relative to $\frac{1}{2}$ O_2, while H_2O binding is relative to H_2O in vacuum.

System	Cu oxidation state	O binding energy (eV)	H_2O binding energy (eV)
Cu(111)	+0.0	-1.36	-0.19
Cu@Cu(111)	+0.11	-1.10	-0.47
Cu@Au(111)	+0.30	-0.05	-0.56
Cu@Al@2*d*-silica	+0.78	0.87	-1.30

Understanding the role of intrinsic surface electrostatics in water-surface bonding

As shown above, the interaction between water and clean TM surfaces is understood based on a *d*-band model. We now turn our attention to other materials where a simple covalent model fails. We find the non-covalent interactions originating from intrinsic surface electrostatics (ISE) to be the dominant interaction. Positive centers (surrounded by negative centers) which form as a result of electron transfer from more electropositive (e.g., metals) to more electronegative constituents of the solid (e.g., O or N in oxides or nitrides, respectively) create strong local electrostatic potential (ESP) wells and strong and inhomogeneous local surface electric fields. These then stabilize the dangling HOMO of H_2O and lead to an "electrostatic bond".

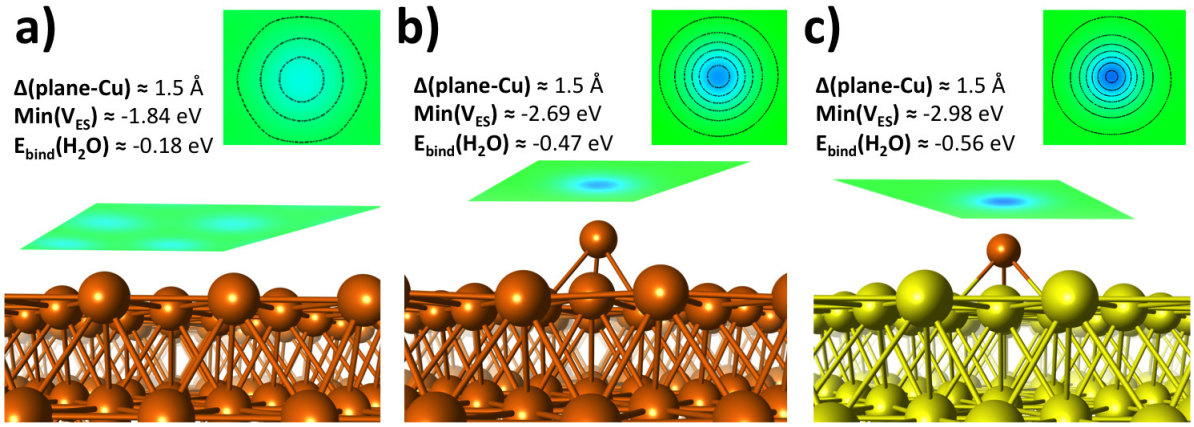

Figure 6: A partial positive charge on Cu in Cu@Cu(111) and Cu@Au(111) leads to the creation of an ESP well above the Cu. The plane at which the ESP is mapped is chosen to be 1.5 Å above the Cu. Min(V_{ES}) shows the depth of the ESP well. The 2-d heat maps show the ESP on a red-green-blue (RGB) coloring scheme where blue shows the minimum of the ESP.

To elucidate this electrostatic effect, we perform a gedankenexperiment. We embed a Cu atom in different host structures, departing gradually from the behavior of clean TMs, and we calculate the oxidation state of the Cu in each structure using Bader charge analysis (BCA)[117,118]. From the data shown in Table 1, the formation of a partial positive charge on

the Cu increases the H_2O BE. First we look at a Cu atom added on Cu(111) and Au(111), denoted by Cu@Cu(111) and Cu@Au(111), respectively. Here, the partial positive charge is formed due to the loss of metal coordination and relative destabilization of the Cu valence orbitals that lead to electron migration to the Fermi energy (the electron sea located on surrounding more coordinated copper atoms). There is a bigger partial charge on Cu adsorbed on Au(111), since in addition to the aforementioned effect, there is also a difference in electronegativity that drives electrons from Cu to the Au(111) bed[119,120]. The greatest partial charge is noticeable on the system in which Cu bonds to electronegative O atoms, denoted by Cu@Al@2d-silica (similar to Cu-exchanged zeolites[121,122]). Figure 6 shows how the partial positive charge creates an ESP well.

To understand how the partial positive charge and the associated ESP well enhance H_2O bonding, we analyze the bonding mechanism on Cu@Au(111). As per Fig. 7, we bring down the H_2O from a larger distance in vacuum to its equilibrium bonding distance. It is seen that as H_2O approaches the surface Cu atom, it feels the ESP well and the strong non-uniform electric field associated with it and its HOMO (depicted in Fig. 2) polarizes[103,124,125], leading to more electron density on the side facing the surface. The fact that H_2O can redistribute its electrons on the side facing the ESP well further stabilizes its bonding, as even more electrons can lower their potential energy in the ESP well. The gradual energy downshift of the H_2O HOMO is evident in Fig. 7 (e). (Some details on the geometry and charge redistribution shown in Fig. 7 are in section 4 of the SI).

Having a simple covalent model (eq. 7) constructed for H_2O on clean TM surfaces allows us to disentangle the covalent effect from the electrostatic effect for H_2O binding to Cu@Au(111). Here, unlike the case of clean TM surfaces, there is an additional contribution to the BE. Thus the right side of eq. 7 does not yield the whole BE, but only the covalent contribution. As seen in Fig. 4 (c), for all surfaces in Table 1, the same covalent contribution to the BE is predicted (the same EBD). Therefore, the difference in H_2O BE for these compounds, from -0.19 for Cu(111) to -1.30 eV for Cu@Al@2d-SiO_2, is due to the difference

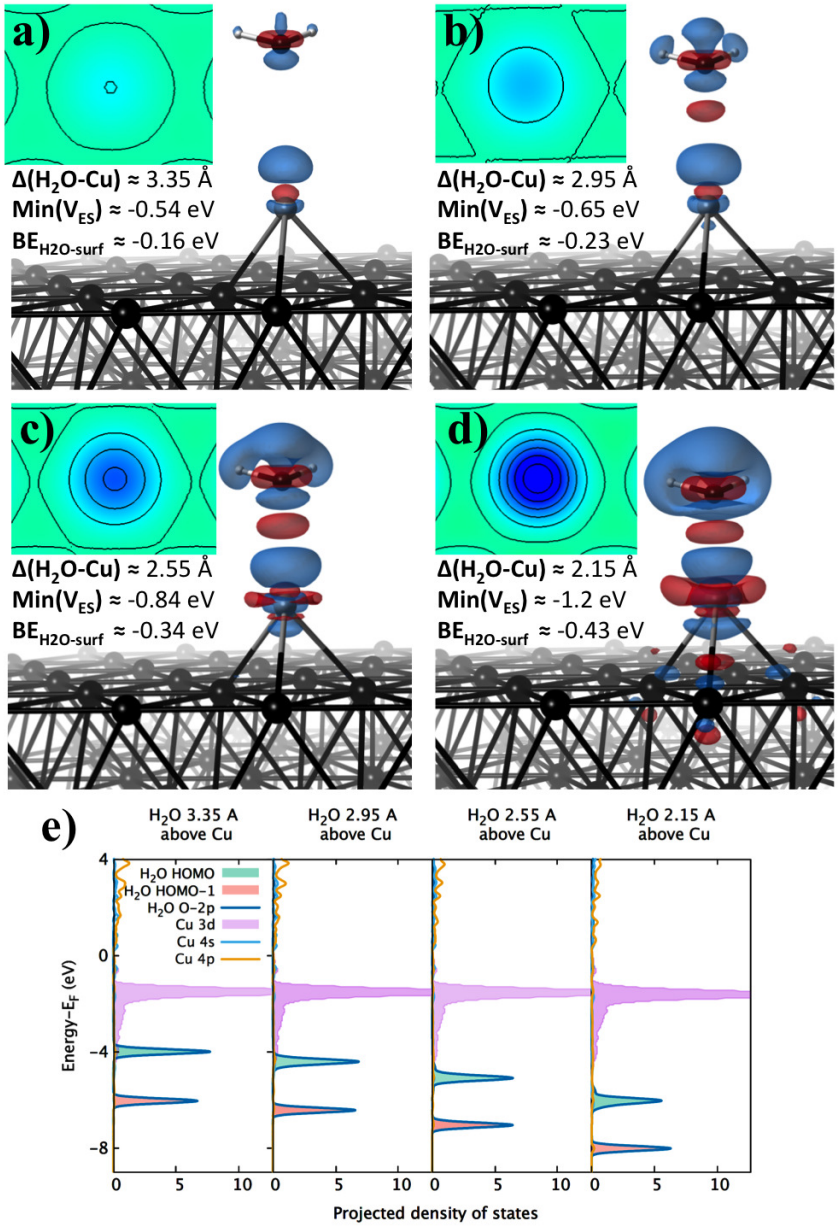

Figure 7: (a) to (d) electron density redistribution ($\rho_{with\ water} - \rho_{water} - \rho_{without\ water}$) as a function of H_2O distance as it approaches the Cu from vacuum to its equilibrium bonding distance on Cu@Au(111). The dangling H_2O HOMO polarizes in response to the ESP well. In the 3-d electron redistribution plots[123] , red (blue) shows the regions (de)populated by electrons, for the same isovalue. The 2-d heat maps show the ESP on an RGB coloring scheme in which blue shows the minimum of the ESP. (e) PDOS. To generate this figure, we first relax the surface geometry with adsorbed (shown in d). We then rigidly displace the H_2O in the z-direction with no further relaxation and perform self-consistent field calculations to obtain the electron density and density of states.

in ISE.

The fact that H_2O BE scales with EBD and center of *d*-band on clean TM surfaces (Fig. 4) is the reason for the H_2O-O scaling on these materials (Figures 4 (a) and 8 (a)). As seen in Fig. 8 (a) the H_2O-O scaling for TM surfaces even holds for calculations done on TM monolayers with only small deviations. The ISE breaks the scaling between *d*-band center and H_2O binding by introducing a more important bonding mechanism. By enhancing ISE one gets more pronounced deviation from H_2O-O scaling line on TM based materials. We designed a numerical experiment to test the effect of extreme ISE using TM-only materials: we took two TMs with extreme electronegativity difference, namely Y and Au[120], and put a single Y atom on top of Au(111) bed (Fig. 8 (c)). BCA shows that the Y acquires a charge of $+1.6\,e$, much greater than Cu partial charge on Cu@Cu(111) and Cu@Au(111). As predicted, Y@Au(111) has the largest deviation from the scaling lines for clean TM surfaces in both Fig. 8 (a) and Fig. 4 (c), a direct result of its sizable ISE. Another set of numerical experiments were done on TM dimers, stripes and clusters on clean facets to elucidate the importance of electrostatics and how it creates deviation from the scaling line in Fig. 8(a). Details on this are in section 5 of the SI.

Looking at the results presented in Table 1, we note the different trends for O and H_2O binding. This is due to two different mechanisms of bonding. For O, we have charge transfer from metallic delocalized *sp* states, while for H_2O, we have HOMO polarization under ISE and an interaction strength depending on the depth of the ESP well. Thus, among systems presented in Table 1, Cu(111) has a relatively strong O binding as *i*) it is a conductor with delocalized *sp* states at the Fermi level, *ii*) it has a small enough work function so that these electrons pour into and stabilize the O-2*p* states. Conversely, Cu@Al@2*d*-SiO_2 is an ionic solid with a bandgap and has a very weak O binding. Nevertheless, it is exactly due to this ionic nature that it has a significant ISE and a strong affinity for H_2O, while Cu(111) has no ISE and very weak affinity for H_2O. The general lack of correlation between H_2O and O binding (beyond clean TM surfaces) is evident in Fig. 4 (a). To reemphasize, all four systems

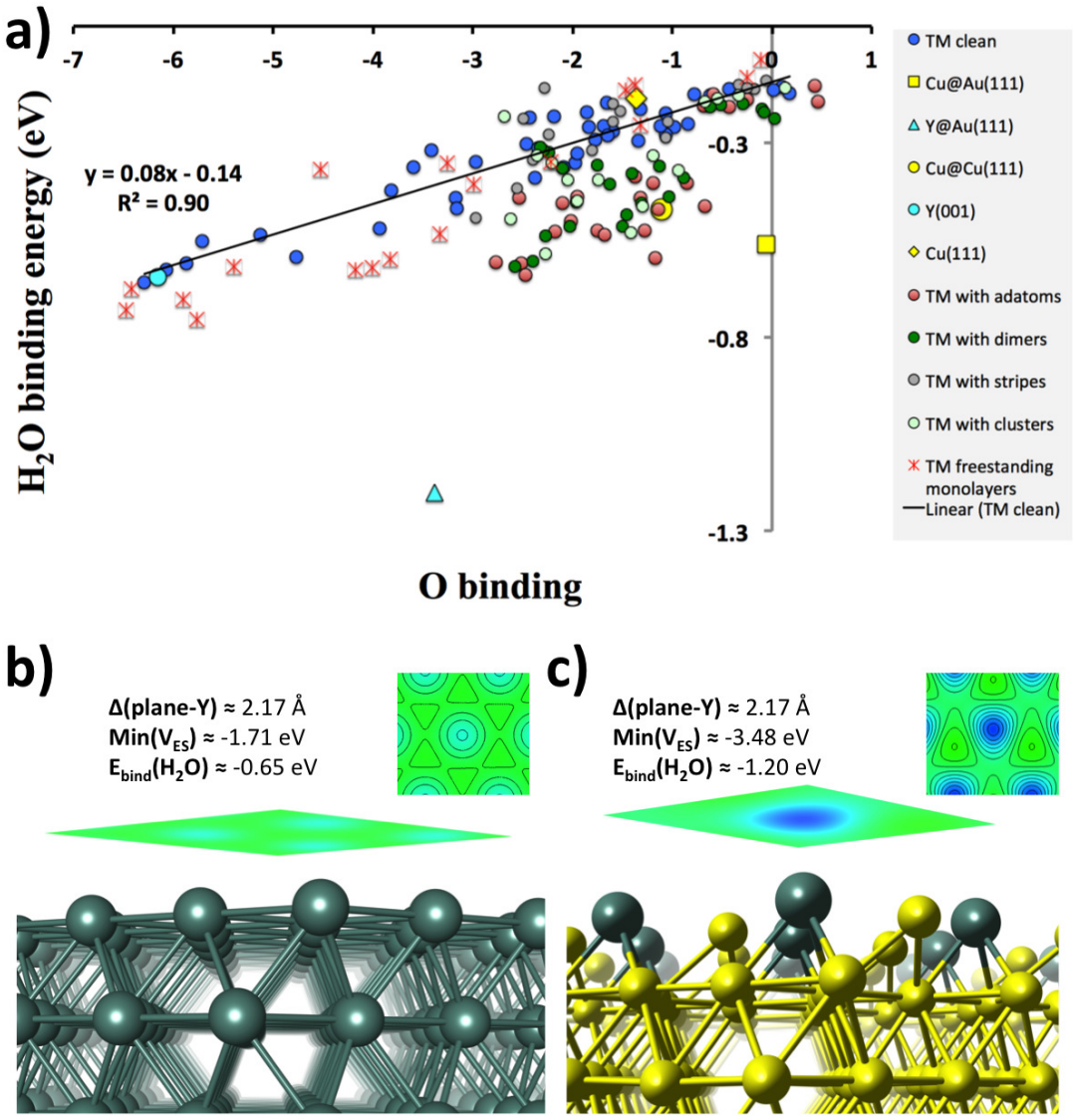

Figure 8: In (a) it is seen how most of the points that deviate from H_2O-O scaling line are adsorbed adatoms, dimers or clusters of TM on clean TM surfaces. Increasing the ISE by depositing a (relatively) electropositive TM atoms on a (relatively) electronegative TM bed leads to bigger deviation from the scaling line. In (b) Y(0001) and in (c) Y@Au(111) is shown. Extreme ISE, H_2O binding, and ESP well are created on Y@Au(111) due to the extreme electronegativity difference among the two elements. This greatly enhances H_2O binding on Y@Au(111) relative to clean Y(0001). On Y@Au(111), major surface reconstructions drag one Au per unit cell out of the plane.

in Table 1, have the same EBD (according to Fig. 4 (c)), thus the same contribution from covalency, so one sees clearly how HOMO polarization and stabilization in ISE-generated ESP well is the dominant effect in H_2O bonding. (A discussion on why embedding the same atom in different environments leads to a larger or smaller change in EBD and H_2O binding is in section 6 of the SI).

Lone-pair bonding beyond transition metal surfaces

The best starting point for understanding water bonding to ionic materials is a metallic system with considerable ionic nature e.g., rutile $IrO_2(110)$ comprised of Ir^{4+} cations and O^{2-} anions. Due to the large positive formal charge on Ir, the $IrO_2(110)$ has a significant ISE, deep ESP wells, and large H_2O BE (-1.39 eV for intact molecular binding). This is a general feature among the rutile XO_2 surfaces for molecular binding of H_2O and molecules which scale with it [20,48,98,126]. The difference between a simple on-top and a more complicated geometry with more significant hydrogen bonding is negligible (see section 7 of the SI). Hence, below we restrict ourselves to on-top binding (with BE of -1.34 as opposed to -1.39 eV) to focus on major electrostatic effects.

In Fig. 9 we look at changes in the electron density distribution as water approaches the metal cation on the $IrO_2(110)$. As the H_2O begins to feel the ESP well, its HOMO begins to polarize and stabilize (downshift in energy evident in Fig. 9 (e)). The broadening of the H_2O HOMO is more significant on $IrO_2(110)$ than on Cu@Au(111) (compare Fig. 9(e) to 7(e)), and this suggests a greater covalent contribution to the BE. This is also confirmed by using eq. 7 and the corresponding EBD values (Fig. 4 (c)) for the two systems. The EBD value for $IrO_2(110)$ yields a value of ≈ -0.5 eV as the covalent contribution (using eq. 7), thus the remainder of the -1.34 eV BE is attributed to the non-covalent electrostatic effect. The covalent contribution is read off from Fig. 4 (c) by drawing a vertical line from the point for $IrO_2(110)$ and finding its intersection with the scaling line. One also observes (Figures 9 (a) to (d)) that as the H_2O approaches the surface, in order to *i*) minimize the electron-electron

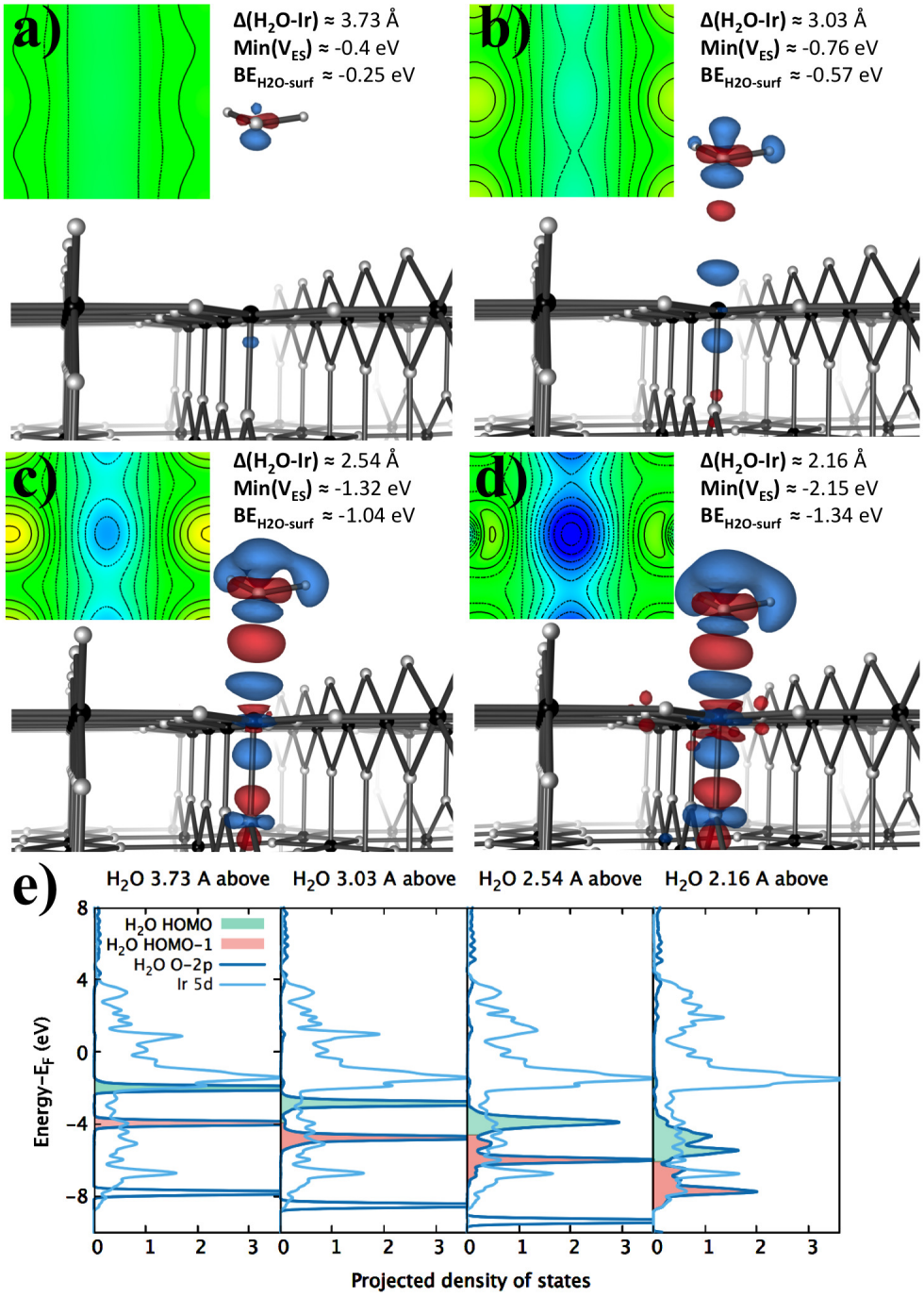

Figure 9: (a) to (d) electron density redistribution as a function of displacing H_2O in z-direction from vacuum to its equilibrium bonding distance on $IrO_2(110)$. In the 3-d electron redistribution plots red (blue) shows the regions (de)populated by electrons. The 2*d* heat maps depict the ESP. (e) PDOS. The lattice oxygens are shown by the small white balls.

repulsion between filled H_2O states and surface states, and *ii*) to create a surface dipole that further enhances the H_2O binding[103], electrons on Ir redistribute (among hybridized states close to E_f) and some migrate to the O below. $IrO_2(110)$ is a metallic surface that has a strong H_2O binding along with a reasonable affinity for O. A side by side analysis which contrasts the charge transfer and covalent nature for O and OH with an electrostatic nature for H_2O bonding on $IrO_2(110)$ is in section 9 of the SI.

The role of geometry in lone-pair bonding

As can be understood from the example of $IrO_2(110)$ and comparison with Cu@Cu(111) and Cu@Au(111), a greater ISE leads to stronger H_2O binding. Nevertheless, ISE does not guarantee a strong interaction with H_2O as surface geometry also matters. To elucidate the role of geometry and how it changes the depth of local ESP wells near the surface, we consider Fig. 10. The BE we calculate for H_2O on MgO(001) is -0.5 eV (experiment is -0.7 eV[48]). For ZnO($10\bar{1}0$) our DFT value is -1.00 eV (in good agreement with computational literature[50,127–129]), while the experiment is -1.17[48]. For IrO_2 our calculated value is -1.4 eV. We note that although our DFT calculated value for MgO and ZnO were underestimated by ≈ 0.2 eV compared to experiment (most probably due to underestimation of the vdW interaction[107,112,130,131]), the difference in H_2O BE for the two is almost in perfect match with experiment, yet another example of DFT capturing BE trends better than their absolute values[132,133].

Comparing our values of -0.5, -1.0 and -1.4 eV for MgO(001), ZnO($10\bar{1}0$) and $IrO_2(110)$, respectively, we ask what determines this hierarchy of the BEs? All three have strong ionic nature, so ISE effects are present for all. We argue that this difference can be understood by considering *i*) cation formal charges, and *ii*) geometry in which the surface cations and anions are arranged. These factors determine the depth of the ESP well above the surface which is the major factor for determining H_2O BE. Comparing Figures 10 (a) and (b), one sees the effect of cation formal charge. On both $IrO_2(110)$ and MgO(001) the cation is sur-

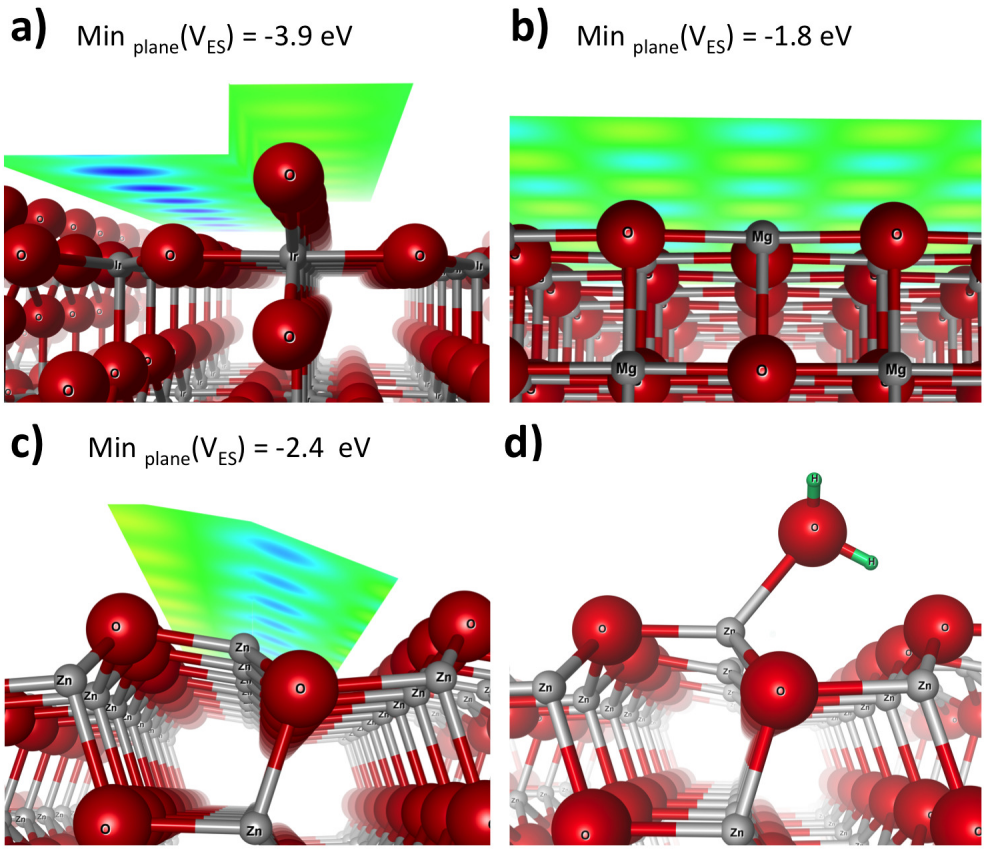

Figure 10: Local ESP wells on the surface of a) $IrO_2(110)$, b) MgO(001), c) $ZnO(10\bar{1}0)$. The planes at which the ESP is plotted are chosen to be (1 Å+cation ionic radius)[134] away from the surface. d) H_2O binding geometry on $ZnO(10\bar{1}0)$. Color code: O (Red) and metal cation (gray).

rounded by four O^{2-} in a (almost) planar geometry. In $IrO_2(110)$, we see a deep ESP well and a strong H_2O binding but not on MgO(001), a difference ascribed to the cation formal charges (Mg^{2+} vs. Ir^{4+}). Comparing Fig. 10 (b) and (c), one observes a deeper ESP well on ZnO (relative to MgO) which causes it to bind H_2O stronger. ZnO and MgO, have the same (+2) cation formal charge: what causes the difference is the different geometry in which the cations and anions are arranged. In $ZnO(10\bar{1}0)$, each Zn^{2+} is surrounded by three O^{2-} and arranged in a geometry in which the Zn sticks out from the oxygens' plane, while for MgO(001) each Mg^{2+} is surrounded by four O^{2-} in a planar geometry, so the proximity of more anions creates a shallower ESP well. One should also note that as depicted in Fig. 10 (d) and consistent with the electrostatics-driven water binding, the H_2O binding geometry to $ZnO(10\bar{1}0)$ surface is angled in a way that the (polarized) HOMO falls into the minimum of surface ESP well.

The cation formal charge has a determining role for H_2O binding to the surface. The anion formal charge is also important. As an example, we have calculated the H_2O BE on $MgF_2(110)$ to be ≈ -1.0 eV, which should be compared to -0.5 eV on MgO(001). In both cases, H_2O binds in an on-top geometry to Mg^{2+}, but for rutile structure $MgF_2(110)$, Mg^{2+} is surrounded by four F^-, while for MgO(001), Mg^{2+} is surrounded by four O^{2-}. Naturally the ESP well is deeper and H_2O BE is larger in magnitude on Mg^{2+} in $MgF_2(110)$. More examples on the effect of geometry on lone-pair bonding (on $\alpha-$ and $\gamma-$alumina and fluorides) are in section 10 of the SI.

For confirmation that the above differences e.g., between H_2O binding on MgO(001) and $IrO_2(110)$, are mostly due to the difference in ISE rather than difference in covalency, see section 11 of the SI.

The role of surface mechanical properties in lone-pair bonding

Having discussed the role of geometry and formal charges, we now move to the effect of surface mechanical properties. They dictate how the surface geometry changes in presence

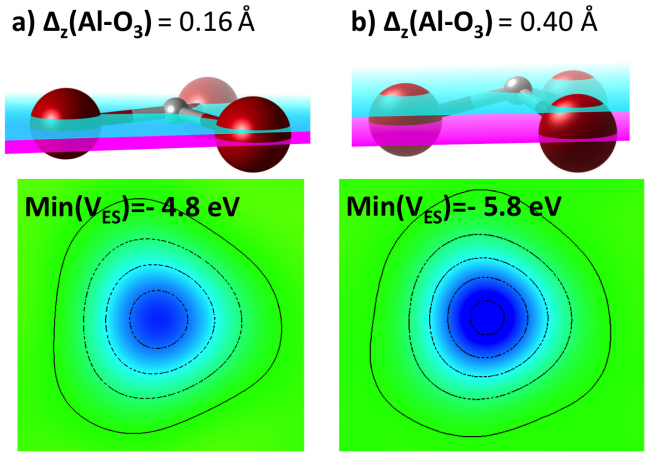

Figure 11: The surface of α-$Al_2O_3(0001)$ mechanically distorts upon H_2O adsorption. a) Al^{3+} cation in its fully relaxed position, b) Al^{3+} cation moving up in presence of H_2O*. The separation between Al^{3+} and O-plane is denoted by $\Delta_z(Al - O_3)$. The planes at which the ESP is plotted are chosen to be $(1\,\mathring{A} + \text{cation ionic radius})$ [134] away from the surface. The minimum of ESP at the plane is denoted by $Min(V_{ES})$.

of the molecular species, and how this effects the BEs.

As seen in Fig. 11 (in agreement with both theory and experiment [135–138]) adsorption of molecular H_2O on Al^{3+} on $\alpha - Al_2O_3(0001)$ leads to an upward shift of Al^{3+} cation. Why does the interaction of a stable closed-shell molecule like water with Al-terminated α-$Al_2O_3(0001)$ surface creates such a large surface distortion? In brief, Al^{3+} movement increases the depth of the ESP well (Fig. 11) and the electrostatic interaction with water HOMO. The stabilization gained by this increased interaction is greater than the mechanical energy cost for the distortion.

Figure 12 shows the interaction and polarization of the H_2O HOMO in the ESP well enhanced by the outward Al^{3+} movement. In Fig. 12 (d), we see accumulation of electrons between Al^{3+} and H_2O, which can be interpreted as a bond formed by the H_2O HOMO getting polarized [103] and its electrons being accumulated on the side facing the surface in response to the strong local electric field generated by the protruding Al^{3+} . BCA reveals that the charge transfer from water to the surface is almost negligible ($\lessapprox 0.01\,e^-$) and all of the electrons, although polarized and shifted toward the surface-facing side of H_2O plane,

still remain within the boundary of H_2O oxygen. This is a sign of a relatively small covalent effect and an electrostatically-driven bond as also confirmed by the PDOS plot in Fig. 12(e) in which the water HOMO and HOMO-1 preserve their relatively sharp molecular nature with just an energy downshift dictated by the ISE and the ESP well it generates. For more details on interpreting Fig. 12(e) see section 12 of the SI.

As an example of how different surface mechanical properties lead to different affinities for binding O and N-2p lone-pair closed shell species, we investigated the effect of doping boron (B) into the α-Al_2O_3(0001) surface: one surface Al out of 4 in a 2×2 cell is replaced by a B. Although B and Al share the same number of valence electrons, B is much smaller[134]. Thus, doping a B in place of an Al leads to stretched and stiffer metal-O bonds which changes the surface's ability to distort. These stiffer B-O are partially responsible for the weaker H_2O BE on B@α-Al_2O_3(0001) ≈ -0.2 eV (compare this to ≈ -1.1 eV on α-Al_2O_3(0001) without B-doping). More details are in section 13 of the SI.

We observe that this type of mechanical distortion, in which the surface cation moves away from the plane of the anions to enhance H_2O BE, is a general behavior[139] for surfaces exposed to water (and other molecules with lone-pair interactions). Some of such distortions are: 0.14 Å for MgO(001), 0.06 Å for IrO_2(110) and 0.01 Å for both Cu@Cu(111) and Cu@Au(111). This "adsorbate-induced lifting" has also been reported in the literature for a number of molecules discussed in this paper including H_2O[137] and CH_3OH[139]. Even for non-ionic surfaces, such a lifting destabilizes the valence orbitals on the "lifted" atoms relative to its neighbors and leads to creation of a partial positive charge on that atom which can stabilize the lone-pair bonding. There is a mechanical cost to create this distortion, but there is a gain by enhancing the lone pair–surface bonding. The interplay of these positive and negative terms determines the exact amount of lifting for each specific case.

As mentioned earlier, rutile-structure XO_2 compounds have a strong affinity for lone-pair bonding. Nevertheless, there is a hierarchy among rutile metal oxides[48]. This can also be related to the different surface mechanical properties (details in section 14 of the SI).

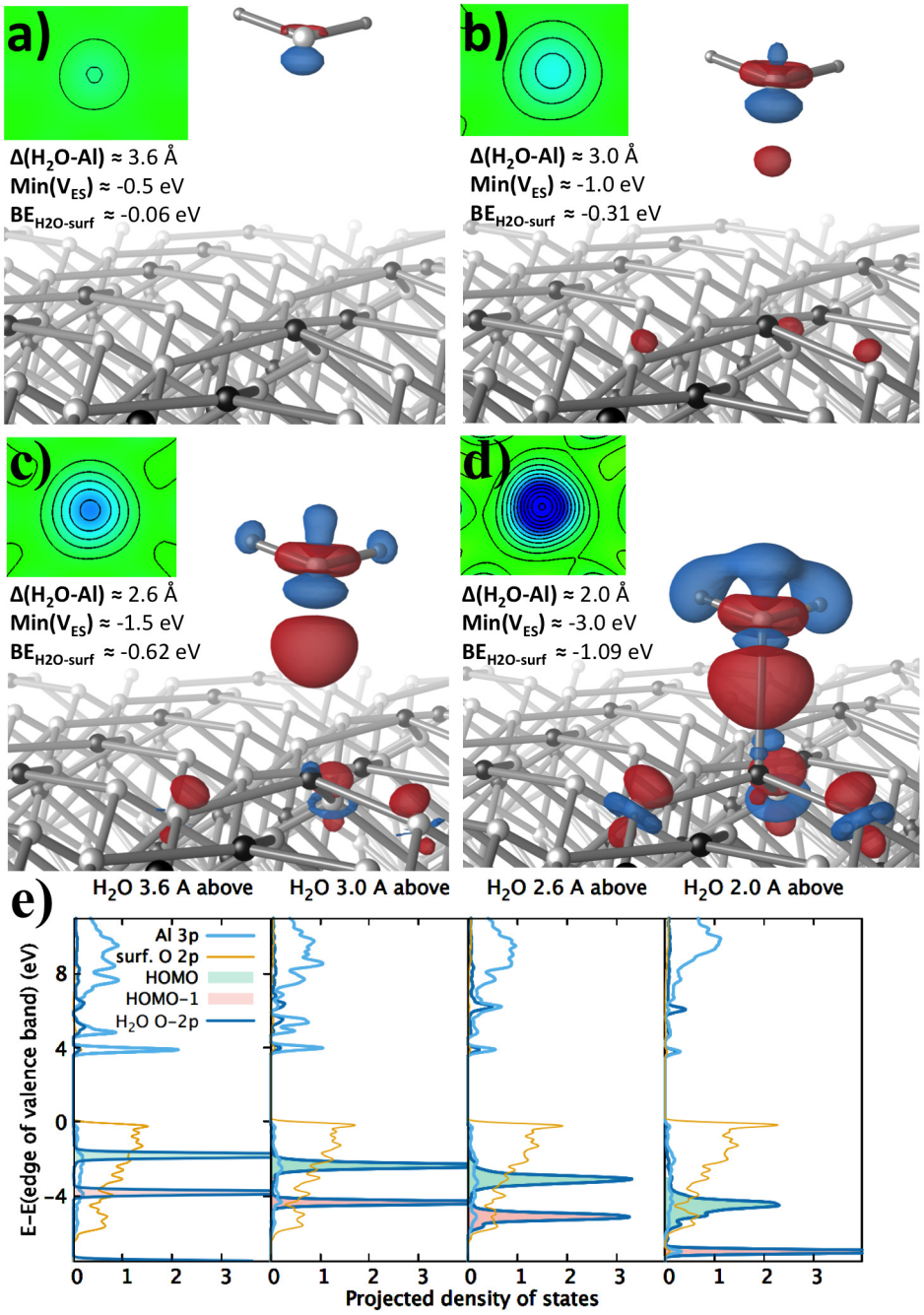

Figure 12: (a) to (d) electron density redistribution as a function of displacing H_2O from vacuum to its equilibrium bonding distance on α-Al_2O_3(0001). In 3-d electron redistribution plots red (blue) shows the regions (de)populated by electrons plotted for the same isovalue. The 2-d heat maps depict the ESP. (e) PDOS.

More details on material-independence of the lone-pair scaling relations

Why is there a material-independent scaling relation for the BEs of N and O-2p lone pair species discussed here? We describe some conjectures below.

There are some common features among this class of molecules: the chemically active part of the molecule (for surface adsorption) is the O (N) atom where the high energy (thus potentially chemically active) and dangling occupied orbitals are located. Also, the HOMOs of this class of molecules are non-bonding MOs dominated by 2p character around N^{3-} or O^{2-} core and are energetically in close proximity (Fig. 2), and thus should share similar polarizabilities. Therefore, from the point of view of the surface, these molecules are very similar. The different sizes of these molecules can lead to different (size-dependent) vdW interactions with the surface[140–143]. Nevertheless, this discrepancy can be adsorbed in the y-intercept of the scaling.

Another common feature in the class is the fully saturated N^{3-} and O^{2-} atoms: the molecules are not in need of any charge transfer from the surface. They only "see" the surface locally through the depth of the ESP well and the center of the empty part of the surface bands. Their binding is not strongly affected by the surface conductivity or the availability of an electron reservoir. This differs from unsaturated (e.g., OH_x ($x < 2$)) species. A gedankenexperiment which contrast the nearsightedness of molecular H_2O binding with more delocalized atomic binding mechanism for O is presented in section 15 of the SI. The effect of this nearsightedness is also evident once one considers the coverage dependence for H_2O binding to surfaces (section 16 and 17 of the SI).

For the molecules discussed here, the O or N (on which the lone-pair is located) is bound via single bonds to neighboring atoms and groups. One might initially think that a molecule like formaldehyde (CH_2O) in which the HOMO has significant O-2p character[144] is also a member of the class of molecules discussed here and scales with the others. This is not the case due to the double bond between C and O (see section 18 of the SI for more details).

A discussion on the possible role of steric hindrance and interaction with multiple sites for the case of larger molecules on corrugated surfaces are in section 19 of the SI.

Dissociative versus intact binding

Throughout this work, we have focused on molecular (as opposed to dissociated) surface binding of closed-shell species. On some surfaces, the molecular binding mode is not the global energy minimum and the molecule prefers to dissociate. This can happen on some metallic compounds with strong affinity for O and OH binding[145,146] or on some ionic insulators[147–150]. Nevertheless, in almost all of these cases, molecular (intact) binding mode exists as a stable local minimum. An interesting question is: when is the dissociated binding more energetically favorable than the intact (molecular) mode? Currently, we do not have a complete answer to this question, but this can be an interesting venue for future research. Below we discuss some conjectures and taking water as an example, make some connections to the literature on dissociative binding of these closed-shell molecules.

On metallic systems due to the existence of an electron sea at Fermi level, the driving force for water dissociation is the charge transfer to dissociation products. Here, the affinity for water dissociation will naturally be correlated with O and OH BE, and for example on clean TM surfaces such affinity increases from the right to the left of the periodic table[145,151]. A recent experimental work by Kiawi et al., on cationic Fe_n^+ (n=6-15) clusters shows a size-dependent water dissociation[152]. This can be partially due to the size-dependent availability of mobile charges. As we showed earlier, on clean TM surface H_2O molecular binding scales with O (and OH) BE; consequently, one can find the energy ordering between dissociative and intact binding modes. In addition, the intact water BE can give us the molecular desorption barrier. By comparing this barrier to the dissociation barrier (scales with water dissociative BE) one can also take into account the kinetics. As a result, one can find the border line at which the surface becomes active toward water dissociation. This border is known in the literature to be Ru(001)[145]. For metallic systems in which ISE is present e.g.,

ionic metals like $IrO_2(110)$, the simple scaling between H_2O and O (and OH) breaks down, thus finding a universal borderline for dissociative versus intact binding is not a trivial task, even on metallic systems. Nevertheless one might be able to develop several materials-class-dependent scalings with associated borderlines.

In contrast to metals, on insulators charge transfer from the surface is not the mechanism behind water dissociation. On those ionic insulators on which water dissociation is more energetically favorable (e.g., clean Al-term α-$Al_2O_3(0001)$ [147,153–156]), the dissociation process can be envisaged as follows: i) water first adsorbs molecularly; the strong electric field created by the positive surface cation significantly polarizes the HOMO, dragging its charge density to one side of the molecule and closer to the surface cation, such a state is a local energy minimum (metastable). ii) A rare event (associated with an energy barrier) can then move the system from this metastable state by reshaping the electron cloud even further such that the whole electron density is taken from the water H atom, forming an OH^- and a H^+ , with H^+ possessing a momentum component moving it away from the local attraction field created by OH^-; the H^+ ejection will then be further facilitated by the strong repelling electric field created by the surface cation and the attractive field of the nearby anion. iii) The ejected H^+ gets attached to the neighboring surface anion. The whole process is a heterolytic bond cleavage. The H^+ attached to the surface anion, is also attracted (via Coulomb interaction) to its OH^- pair on the neighboring surface cation: this can lead to large energy costs to further separate them [157,158]; this is also known in the literature as acid-base stabilization [159,160]. The most important interactions for such a dissociated binding mode can be thought of as: i) the OH^- –surface cation, ii) the H^+ –surface anion, and iii) the H^+–OH^- interaction. The question of which binding mode (intact versus dissociative) is more stable, then reduces to: when is the collective effect of the three aforementioned interactions stronger than the H_2O lone pair–surface bond? We conjecture that the OH^-–surface cation interaction in such systems can, in principle, scale with the molecular H_2O BE on these surfaces, as an OH^- is isoelectronic to H_2O. This scaling can create a correlation between H_2O molecular and

dissociative binding modes on ionic insulators.

As mentioned before, there are a subset of ionic systems which are metallic or there exist metallic states in their immediate neighborhood. An interesting observation is that such metallic states can further stabilize the dissociation mode on these materials. Few examples include enhancement of water dissociation on i) metallic[161] (CaO terminated) $Ca_3Ru_2O_7(001)$ relative to the insulator $CaO(001)$[162], on ii) MgO ultrathin layers on metallic supports (with or without interfacial defects)[163–165] and on iii) (polarization-driven) charge-doped ferroelectric oxide surfaces e.g., $PbTiO_3(001)$[166].

Lewis acid and base concepts revisited for surface chemistry

We have introduced scaling relations between molecules which interact with the surface through their $2p$-lone-pairs. In molecular chemistry, these are categorized as Lewis bases (LB). Similarly, the surface sites which bind these molecules are Lewis acid (LA). In a standard Lewis acid-base interaction (LABI), it is often assumed that the HOMO of the LB covalently interacts with the LUMO of the LA to create a lower energy level for the electron pair to occupy. Since this lower energy state is a mixture of LB HOMO and LA LUMO, this leads to an effective charge transfer from the LB to LA.

In 1982 Stair applied the Lewis acid and base concept to the study of surface chemical phenomena[167]. Using the perturbational molecular orbital theory of acid-base interactions developed by Klopman[168] and extended by Jensen[169], the perturbation energy ΔE^{pert} is:

$$\Delta E^{pert} = \Delta E^{ch} + \Delta E^{orb} + \Delta E^{repl} \tag{8}$$

Here, ΔE^{repl} is a repulsive term due to the electron-electron repulsion between the filled orbitals. ΔE^{orb} is an attractive term describing the covalent interaction between the LB HOMO and the LA LUMO, similar in nature to the bond energy predicted by the Newns-Anderson Model (eq. 3 and 7). ΔE^{ch} describes the Coulomb attraction between cation

acids and anion bases: for gas phase species it includes permanent dipole, charge-induced-dipole and polarization in addition to charge-charge interactions. According to Stair, this electrostatic interaction is expected to be very weak for neutral acid-base adducts such as molecules bonded to a surface, so the electron transfer via covalent bonding accounts for the LABI in surface chemistry. Some of the surface phenomena discussed in this work agree with this fully-covalent picture but most require modifications to it.

The natural re-definition of a LUMO for surface chemistry is the empty part of the surface chemically active band (SCAB); for TMs this is the empty part of the *d*-band. For TM surfaces, we showed that the surface–water interaction is captured by a simple covalent model (eq. 7). According to the mutual scalings between water and the other molecules in the class, similar models can be made for the rest of them. The picture of a fully covalent interaction works well for clean TM surfaces. Looking at Fig. 1 and the scaling equations, one notices that generally $|BE(\mathrm{H_2O})| < |BE(\mathrm{CH_3OH})| < |BE(\mathrm{NH_3})|$, this can be rationalized by a fully-covalent LABI picture considering the HOMO alignment of these molecules (Fig. 2), $E_{HOMO}(\mathrm{H_2O}) < E_{HOMO}(\mathrm{CH_3OH}) < E_{HOMO}(\mathrm{NH_3})$. A higher HOMO energy means a stronger covalent interaction with the surface, as the HOMO gets closer to the empty part of the SCAB. Although this BEs trend can be justified within a fully covalent picture, there is yet another contributing phenomenon working in the same direction that has an electrostatic rather than covalent origin: a higher energy HOMO is easier to polarize and responds better to the surface ESP well. An example investigating NH_3 binding to an oxide surface, illustrating its similarities and differences compared to the H_2O binding is in section 20 of the SI.

Another qualitative agreement with a fully covalent LABI picture is our prediction of the surface active sites for lone-pair bonding. The LB species prefer to bond to surface atoms that dominate the empty part of the SCAB, i.e., surface LA site, the atom with a higher electropositivity[29]. In a standard fully covalent LABI picture, this causes a better overlap between filled LB and empty LA orbitals. Another reason, based on results and

discussions in our work, is that these types of sites have some partial positive charge leading to an ESP well which electrostatically polarizes and stabilizes the HOMO. Based on our calculations, the class of closed-shell molecules discussed here always bind preferably to the most electropositive surface constituent even when the difference of electronegativity is small[170–174] (examples in section 21 of the SI).

Beyond the simple case of clean TM surfaces, the simple fully covalent LABI picture is insufficient to describe the lone pair–surface bonding. Taking Cu as an example, we showed (Fig. 4(c)) how creation of ISE changes the lone-pair BE to the surface without changing the EBD (eq. 7): with the same covalent contribution, a positive center creates an ESP well, polarize the dangling HOMO and create a stronger lone pair–surface bond. This is not a chemical bond as it is not associated with considerable mixing among surface and adsorbate states, nor is there a considerable charge transfer from the molecule to the surface. As indicated by BCA, the HOMO polarization which results in electron accumulation between H_2O and the surface site does not involve any sizable charge transfer to the surface LA site: the lone-pair electrons polarize but remain within the H_2O. The small numbers reported in this work (few hundredth of e^-) for charge transfer from LB to surface LA site are a result of the covalent interaction of LB HOMO and surface LA LUMO (empty part of surface effective band), not the HOMO polarization. Our work on TM adatoms on TM clean surfaces and oxides shows that the extent of the effect of ISE-driven HOMO polarization and stabilization can be larger than the covalent contribution. Thus on many surfaces with strong affinity for lone-pair (molecular) bonding, the bond is characterized as a strong physical (electrostatic) rather than a chemical (covalent) bond: the attractive contribution of ΔE^{ch} in eq. (8) is significant.

The surface binding of the class of closed shell molecules discussed in this work, has been frequently named in the literature as a dative bond[21,127,137,175–189]. Throughout this work, we intentionally refrained to use this term, as a dative bond is a type of covalent bond, while our results show that the covalent effect does not, in general, fully capture the nature of the

lone pair–surface bonds.

Taking into account both electrostatic and covalent contributions to the BEs also allows for rationalization of the lone pair–surface binding geometries (section 22 of the SI).

Outlook and Conclusions

Scaling relations among the binding energies (BEs) of $AH_x (x < x_{max})$ species have been shown to exist[1,190,191] and have become a cornerstone of theoretical catalyst design[2,192–194]. We have expanded the reaches of this approach, by demonstrating material-independent scaling relations among some species with $x = x_{max}$, such as H_2O and NH_3, and other similar closed-shell lone-pair species including alcohols, ethers and amines. We showed, in general, a lack of correlation between the molecular BEs of these saturated X_{max} species (e.g., H_2O) and their open-shell relatives (e.g., O), except for special cases such as binding to clean TM surfaces. Electron transfer from the surface to adsorbate is the major contributor for effective binding of AH_x $(x < x_{max})$ species. This mechanism is non-existent for closed-shell lone-pair species discussed here. Hence, one has the freedom to engineer the materials properties and tune these two type of BEs independently. For instance, a metallic TM surface is active toward O and inert toward intact molecular adsorption of H_2O, while an insulating ionic system can be active toward H_2O and inert toward O. The illustration of this apparent lack of correlation between the surface chemistry of closed-shell molecules and their radical dehydrogenated relatives provides new ideas and insights for catalytic materials design. One possible application is designing hybrid systems with sites that are active toward radicals but inert toward closed-shells and vice versa.

Having identified material-independent correlations among this class of closed-shell molecules, we described the bonding mechanism for H_2O the findings of which are generalizable to the other molecules. We explained the critical role of intrinsic surface electrostatics (ISE) in creating local electrostatic potential wells which polarize and stabilize the dangling lone-pair

(HOMO) of these molecules. For cases of strong bonding, this electrostatic effect was shown to be the dominant interaction. The role of surface electronic structure, geometry, formal charges, and mechanical properties in dictating the strength of lone pair–surface bond were also investigated. This fundamental understanding was used to explain the wide span of the BEs both experimentally and computationally observed on different categories of materials[44,48]. For instance, we discussed why lone-pair molecular binding is generally weaker on clean transition metals and stronger on ionic oxides or why there is a hierarchy even within ionic materials class[48]. Other experimental observations including adsorbate-induced lifting of surface cations in ionic solids[135–139] were also elucidated. We have also related our findings on solid-state systems to the general Lewis acid-base interactions in the context of molecular chemistry. The insights garnered here lets us expand the scaling-driven catalyst discovery approach[2,3,195,196] to include an important class of closed-shell molecules.

Abbreviations

DFT, Density Functional Theory; BE, binding energy; MO, molecular orbital; HOMO, highest occupied molecular orbital; LUMO, lowest unoccupied molecular orbital; TM, transition metal; EBD, empty band descriptor; SCAB, surface chemically active orbital; ISE, intrinsic surface electrostatics; PDOS, projected density of states; ESP, electrostatic potential; BCA, Bader charge analysis; LABI, Lewis acid-base interaction; LA, Lewis acid; LB, Lewis base

Computational Methods

We performed calculations using Density Functional Theory (DFT)[197,198] with plane wave basis sets, mostly using the Quantum Espresso software package[199]. The Bayesian error-estimation functional with van der Waals interactions (BEEF-vdW)[133] was used as the exchange correlation functional. Details on convergence parameters and pseudo potentials used in different sets of our calculations are in section 23 of the SI. The convention for the sign

of the BEs is that an exothermic process corresponds to a negative adsorption energy. For instance, water BEs are defined as:

$$BE(\mathrm{H_2O}) = E_{\mathrm{bind}}(\mathrm{H_2O}) = E(\text{Surface with } \mathrm{H_2O}) - E(\text{bare surface}) - E(\mathrm{H_2O} \text{ molecule})$$

Associated Content

The Supporting Information document associated with this article contains details including the list of materials and BEs used in this work.

Author Information

corresponding Author:

Jens K. Nørskov: norskov@stanford.edu

Notes:

The authors declare no competing financial interest

Acknowledgements

Support from the Global Climate & Energy Project (GCEP) and the U.S. Department of Energy Office of Basic Energy Science to the SUNCAT Center for Interface Science and Catalysis is gratefully acknowledged. We thank Dr. Johannes Voss and Dr. Cina Foroutan-Nejad for useful discussions as well as the Stanford Research Computing Center for HPC computing help and support. Ismail-Beigi was supported by the NSF via grant MRSEC DMR-1119826.

References

(1) Abild-Pedersen, F.; Greeley, J.; Studt, F.; Rossmeisl, J.; Munter, T. R.; Moses, P. G.; Skulason, E.; Bligaard, T.; Norskov, J. K. Scaling Properties of Adsorption Energies for Hydrogen-Containing Molecules on Transition-Metal Surfaces. *Phys. Rev. Lett.* **2007**, *99*, 016105.

(2) Vojvodic, A.; Norskov, J. K. New design paradigm for heterogeneous catalysts. *Natl. Sci. Rev.* **2015**, *2*, 140–143.

(3) Greeley, J. Theoretical Heterogeneous Catalysis: Scaling Relationships and Computational Catalyst Design. *Annu. Rev. Chem. Biomol. Eng.* **2016**, *7*, 605–635.

(4) Liu, B.; Zhou, M.; Chan, M. K. Y.; Greeley, J. P. Understanding Polyol Decomposition on Bimetallic Pt–Mo Catalysts—A DFT Study of Glycerol. *ACS Catal.* **2015**, *5*, 4942–4950.

(5) Wang, Z.; Zhao, J.; Cai, Q.; Li, F. Computational screening for high-activity MoS 2 monolayer-based catalysts for the oxygen reduction reaction via substitutional doping with transition metal. *J. Mater. Chem. A* **2017**, *5*, 9842–9851.

(6) Ulissi, Z. W.; Medford, A. J.; Bligaard, T.; Nørskov, J. K. To address surface reaction network complexity using scaling relations machine learning and DFT calculations. *Nat. Commun.* **2017**, *8*, 14621.

(7) Latimer, A. A.; Kulkarni, A. R.; Aljama, H.; Montoya, J. H.; Yoo, J. S.; Tsai, C.; Abild-Pedersen, F.; Studt, F.; Norskov, J. K. Understanding trends in C–H bond activation in heterogeneous catalysis. *Nat. Mater.* **2017**, *16*, 225.

(8) A. Latimer, A.; Aljama, H.; Kakekhani, A.; Suk Yoo, J.; Kulkarni, A.; Tsai, C.; Garcia-Melchor, M.; Abild-Pedersen, F.; K. Norskov, J. Mechanistic insights into heterogeneous methane activation. *Phys. Chem. Chem. Phys.* **2017**, *19*, 3575–3581.

(9) Remsing, R. C.; Duignan, T. T.; Baer, M. D.; Schenter, G. K.; Mundy, C. J.; Weeks, J. D. Water Lone Pair Delocalization in Classical and Quantum Descriptions of the Hydration of Model Ions. *J. Phys. Chem. B* **2018**, *DOI: 10.1021/acs.jpcb.7b10722*.

(10) Jungwirth, P. Biological Water or Rather Water in Biology? *J. Phys. Chem. Lett.* **2015**, *6*, 2449–2451.

(11) Valero-González, J.; Leonhard-Melief, C.; Lira-Navarrete, E.; Jiménez-Osés, G.; Hernández-Ruiz, C.; Pallarés, M. C.; Yruela, I.; Vasudevan, D.; Lostao, A.; Corzana, F.; Takeuchi, H.; Haltiwanger, R. S.; Hurtado-Guerrero, R. A proactive role of water molecules in acceptor recognition by protein *O*-fucosyltransferase 2. *Nat. Chem. Biol.* **2016**, *12*, 240.

(12) Andersson, J.; Lundgren, J. Techno-economic analysis of ammonia production via integrated biomass gasification. *Appl. Energy* **2014**, *130*, 484–490.

(13) Sun, J.; Yang, G.; Yoneyama, Y.; Tsubaki, N. Catalysis Chemistry of Dimethyl Ether Synthesis. *ACS Catal.* **2014**, *4*, 3346–3356.

(14) Seminovski, Y.; Tereshchuk, P.; Kiejna, A.; Da Silva, J. L. F. The role of the cationic Pt sites in the adsorption properties of water and ethanol on the Pt4/Pt(111) and Pt4/CeO2(111) substrates: A density functional theory investigation. *J. Chem. Phys.* **2016**, *145*, 124709.

(15) Zibordi-Besse, L.; Tereshchuk, P.; Chaves, A. S.; Da Silva, J. L. F. Ethanol and Water Adsorption on Transition-Metal 13-Atom Clusters: A Density Functional Theory Investigation within van der Waals Corrections. *J. Phys. Chem. A* **2016**, *120*, 4231–4240.

(16) H. Freire, R. L.; Kiejna, A.; Silva, J. L. F. D. Adsorption of water and ethanol on noble and transition-metal substrates: a density functional investigation within van der Waals corrections. *Phys. Chem. Chem. Phys.* **2016**, *18*, 29526–29536.

(17) Sutton, J. E.; Vlachos, D. G. Ethanol Activation on Closed-Packed Surfaces. *Ind. Eng. Chem. Res.* **2015**, *54*, 4213–4225.

(18) Du, P.; Wu, P.; Cai, C. Mechanistic Insight into the Facet-Dependent Adsorption of Methanol on a Pt3Ni Nanocatalyst. *J. Phys. Chem. C* **2015**, *119*, 18352–18363.

(19) Senftle, T. P.; Lessio, M.; Carter, E. A. Interaction of Pyridine and Water with the Reconstructed Surfaces of GaP(111) and CdTe(111) Photoelectrodes: Implications for CO2 Reduction. *Chem. Mater.* **2016**, *28*, 5799–5810.

(20) N. Muir, J.; Choi, Y.; Idriss, H. Computational study of ethanol adsorption and reaction over rutile TiO 2 (110) surfaces. *Phys. Chem. Chem. Phys.* **2012**, *14*, 11910–11919.

(21) Chiang, H.-N.; Nachimuthu, S.; Cheng, Y.-C.; Damayanti, N. P.; Jiang, J.-C. A DFT study of ethanol adsorption and decomposition on α-Al2O3(0001) surface. *Appl. Surf. Sci.* **2016**, *363*, 636–643.

(22) Tereshchuk, P.; Da Silva, J. L. F. Density Functional Investigation of the Adsorption of Ethanol-Water Mixture on the Pt(111) Surface. *J. Phys. Chem. C* **2013**, *117*, 16942–16952.

(23) Bedolla, P. O.; Feldbauer, G.; Wolloch, M.; Eder, S. J.; Dörr, N.; Mohn, P.; Redinger, J.; Vernes, A. Effects of van der Waals Interactions in the Adsorption of Isooctane and Ethanol on Fe(100) Surfaces. *J. Phys. Chem. C* **2014**, *118*, 17608–17615.

(24) Erdogan, R.; Ozbek, O.; Onal, I. A periodic DFT study of water and ammonia adsorption on anatase TiO2 (001) slab. *Surf. Sci.* **2010**, *604*, 1029–1033.

(25) Suzuki, K.; Sastre, G.; Katada, N.; Niwa, M. Periodic DFT Calculation of the Energy

of Ammonia Adsorption on Zeolite Brønsted Acid Sites to Support the Ammonia IRMS–TPD Experiment. *Chem. Lett.* **2009**, *38*, 354–355.

(26) Ahmadi, A.; Beheshtian, J.; Hadipour, N. L. Chemisorption of NH3 at the open ends of boron nitride nanotubes: a DFT study. *Struct. Chem.* **2011**, *22*, 183–188.

(27) Isvoranu, C.; Wang, B.; Ataman, E.; Schulte, K.; Knudsen, J.; Andersen, J. N.; Bocquet, M.-L.; Schnadt, J. Ammonia adsorption on iron phthalocyanine on Au(111): Influence on adsorbate–substrate coupling and molecular spin. *J. Chem. Phys.* **2011**, *134*, 114710.

(28) Cheng, D.; Lan, J.; Cao, D.; Wang, W. Adsorption and dissociation of ammonia on clean and metal-covered TiO2 rutile (110) surfaces: A comparative DFT study. *Appl. Catal., B* **2011**, *106*, 510–519.

(29) Dzade, N. Y.; Roldan, A.; de Leeuw, N. H. DFT-D2 simulations of water adsorption and dissociation on the low-index surfaces of mackinawite (FeS). *J. Chem. Phys.* **2016**, *144*, 174704.

(30) Riefer, A.; Sanna, S.; Schmidt, W. G. Polarization-dependent methanol adsorption on lithium niobate Z-cut surfaces. *Phys. Rev. B* **2012**, *86*, 125410.

(31) Grabow, L. C.; Studt, F.; Abild-Pedersen, F.; Petzold, V.; Kleis, J.; Bligaard, T.; Nørskov, J. K. Descriptor-Based Analysis Applied to HCN Synthesis from NH3 and CH4. *Angew. Chem. Int. Ed.* **2011**, *50*, 4601–4605.

(32) Wang, C.-M.; Brogaard, R. Y.; Weckhuysen, B. M.; Nørskov, J. K.; Studt, F. Reactivity Descriptor in Solid Acid Catalysis: Predicting Turnover Frequencies for Propene Methylation in Zeotypes. *J. Phys. Chem. Lett.* **2014**, *5*, 1516–1521.

(33) Brogaard, R. Y.; Wang, C.-M.; Studt, F. Methanol–Alkene Reactions in Zeotype Acid

Catalysts: Insights from a Descriptor-Based Approach and Microkinetic Modeling. *ACS Catal.* **2014**, *4*, 4504–4509.

(34) Calle-Vallejo, F.; Díaz-Morales, O. A.; Kolb, M. J.; Koper, M. T. M. Why Is Bulk Thermochemistry a Good Descriptor for the Electrocatalytic Activity of Transition Metal Oxides? *ACS Catal.* **2015**, *5*, 869–873.

(35) Siahrostami, S.; Vojvodic, A. Influence of Adsorbed Water on the Oxygen Evolution Reaction on Oxides. *J. Phys. Chem. C* **2015**, *119*, 1032–1037.

(36) Khaled, K. F. Corrosion control of copper in nitric acid solutions using some amino acids – A combined experimental and theoretical study. *Corros. Sci.* **2010**, *52*, 3225–3234.

(37) Verners, O.; van Duin, A. C. T. Comparative molecular dynamics study of fcc-Ni nanoplate stress corrosion in water. *Surf. Sci.* **2015**, *633*, 94–101.

(38) Freitas, R. R. Q.; Rivelino, R.; de Brito Mota, F.; de Castilho, C. M. C. Dissociative Adsorption and Aggregation of Water on the Fe(100) Surface: A DFT Study. *J. Phys. Chem. C* **2012**, *116*, 20306–20314.

(39) Castelli, I. E.; Thygesen, K. S.; Jacobsen, K. W. Calculated Pourbaix Diagrams of Cubic Perovskites for Water Splitting: Stability Against Corrosion. *Top. Catal.* **2014**, *57*, 265–272.

(40) Ogasawara, H.; Brena, B.; Nordlund, D.; Nyberg, M.; Pelmenschikov, A.; Pettersson, L. G. M.; Nilsson, A. Structure and Bonding of Water on Pt(111). *Phys. Rev. Lett.* **2002**, *89*, 276102.

(41) Carrasco, J.; Hodgson, A.; Michaelides, A. A molecular perspective of water at metal interfaces. *Nat. Mater.* **2012**, *11*, 667.

(42) Haq, S.; Clay, C.; Darling, G. R.; Zimbitas, G.; Hodgson, A. Growth of intact water ice on Ru(0001) between 140 and 160 K: Experiment and density-functional theory calculations. *Phys. Rev. B* **2006**, *73*, 115414.

(43) Taylor, C. D.; Neurock, M. Theoretical insights into the structure and reactivity of the aqueous/metal interface. *Curr. Opin. Solid State Mater. Sci.* **2005**, *9*, 49–65.

(44) Meng, S.; Wang, E. G.; Gao, S. Water adsorption on metal surfaces: A general picture from density functional theory studies. *Phys. Rev. B* **2004**, *69*, 195404.

(45) Nilsson, A.; Pettersson, L. G. M. *Chemical Bonding at Surfaces and Interfaces*; Elsevier: Amsterdam, 2008; pp 57–142.

(46) Tang, Q.-L.; Chen, Z.-X. Density functional slab model studies of water adsorption on flat and stepped Cu surfaces. *Surf. Sci.* **2007**, *601*, 954–964.

(47) Liu, R. Adsorption and dissociation of H2O on Au(111) surface: A DFT study. *Comput. Theor. Chem.* **2013**, *1019*, 141–145.

(48) Campbell, C. T.; Sellers, J. R. V. Enthalpies and Entropies of Adsorption on Well-Defined Oxide Surfaces: Experimental Measurements. *Chem. Rev.* **2013**, *113*, 4106–4135.

(49) Schiros, T.; Haq, S.; Ogasawara, H.; Takahashi, O.; Ostrom, H.; Andersson, K.; Pettersson, L. G. M.; Hodgson, A.; Nilsson, A. Structure of water adsorbed on the open Cu(110) surface: H-up, H-down, or both? *Chem. Phys. Lett.* **2006**, *429*, 415–419.

(50) Meyer, B.; Rabaa, H.; Marx, D. Water adsorption on ZnO(1010): from single molecules to partially dissociated monolayers. *Phys. Chem. Chem. Phys.* **2006**, *8*, 1513–1520.

(51) Wan, C.-Q.; Chen, X.-D.; W. Mak, T. C. Supramolecular frameworks assembled via intermolecular lone pair-aromatic interaction between carbonyl and pyridyl groups. *CrystEngComm* **2008**, *10*, 475–478.

(52) Otero-de-la Roza, A.; R. Johnson, E.; Contreras-García, J. Revealing non-covalent interactions in solids: NCI plots revisited. *Phys. Chem. Chem. Phys.* **2012**, *14*, 12165–12172.

(53) J. Mooibroek, T.; Gamez, P.; Reedijk, J. Lone pair–π interactions: a new supramolecular bond? *CrystEngComm* **2008**, *10*, 1501–1515.

(54) J. Mooibroek, T.; Gamez, P. Anion– arene and lone pair–arene interactions are directional. *CrystEngComm* **2012**, *14*, 1027–1030.

(55) Das, A.; Ray Choudhury, S.; Estarellas, C.; Dey, B.; Frontera, A.; Hemming, J.; Helliwell, M.; Gamez, P.; Mukhopadhyay, S. Supramolecular assemblies involving anion–π and lone pair–π interactions: experimental observation and theoretical analysis. *CrystEngComm* **2011**, *13*, 4519–4527.

(56) Grimme, S.; Mück-Lichtenfeld, C.; Antony, J. Analysis of non-covalent interactions in (bio)organic molecules using orbital-partitioned localized MP2. *Phys. Chem. Chem. Phys.* **2008**, *10*, 3327–3334.

(57) Zuend, S. J.; Jacobsen, E. N. Mechanism of Amido-Thiourea Catalyzed Enantioselective Imine Hydrocyanation: Transition State Stabilization via Multiple Non-Covalent Interactions. *J. Am. Chem. Soc.* **2009**, *131*, 15358–15374.

(58) Zondlo, N. J. Non-covalent interactions: Fold globally, bond locally. *Nat. Chem. Biol.* **2010**, *6*, 567.

(59) Badri, Z.; Foroutan-Nejad, C.; Kozelka, J.; Marek, R. On the non-classical contribution in lone-pair–π interaction: IQA perspective. *Phys. Chem. Chem. Phys.* **2015**, *17*, 26183–26190.

(60) Chaudret, R.; Courcy, B. d.; Contreras-García, J.; Gloaguen, E.; Zehnacker-Rentien, A.; Mons, M.; Piquemal, J.-P. Unraveling non-covalent interactions within

flexible biomolecules: from electron density topology to gas phase spectroscopy. *Phys. Chem. Chem. Phys.* **2014**, *16*, 9876–9891.

(61) Mohan, N.; H. Suresh, C.; Kumar, A.; R. Gadre, S. Molecular electrostatics for probing lone pair–π interactions. *Phys. Chem. Chem. Phys.* **2013**, *15*, 18401–18409.

(62) Quiñonero, D.; Estarellas, C.; Frontera, A.; Deyà, P. M. A methodological analysis for the assessment of non-covalent π interactions. *Chem. Phys. Lett.* **2011**, *508*, 144–148.

(63) Neel, A. J.; Hilton, M. J.; Sigman, M. S.; Toste, F. D. Exploiting non-covalent π interactions for catalyst design. *Nature* **2017**, *543*, 637.

(64) Mooibroek, T. J.; Gamez, P.; Reedijk, J. Lone pair–π interactions: a new supramolecular bond? *CrystEngComm* **2008**, *10*, 1501–1515.

(65) Ran, J.; Hobza, P. On the Nature of Bonding in Lone Pair$\cdots\pi$-Electron Complexes: CCSD(T)/Complete Basis Set Limit Calculations. *J. Chem. Theory Comput.* **2009**, *5*, 1180–1185.

(66) Gadre, S. R.; Kumar, A. *Noncovalent Forces*; Challenges and Advances in Computational Chemistry and Physics; Springer, Cham, 2015; pp 391–418.

(67) Orlandi, M.; Coelho, J. A. S.; Hilton, M. J.; Toste, F. D.; Sigman, M. S. Parametrization of Non-covalent Interactions for Transition State Interrogation Applied to Asymmetric Catalysis. *J. Am. Chem. Soc.* **2017**, *139*, 6803–6806.

(68) D. Nielsen, M.; Ozolins, V.; P. Heremans, J. Lone pair electrons minimize lattice thermal conductivity. *Energy Environ. Sci.* **2013**, *6*, 570–578.

(69) Leed, E. A.; Sofo, J. O.; Pantano, C. G. Electronic structure calculations of physisorption and chemisorption on oxide glass surfaces. *Phys. Rev. B* **2005**, *72*, 155427.

(70) Gohda, Y.; Schnur, S.; Groß, A. Influence of water on elementary reaction steps in electrocatalysis. *Faraday Discuss.* **2009**, *140*, 233–244.

(71) Liao, P.; Keith, J. A.; Carter, E. A. Water Oxidation on Pure and Doped Hematite (0001) Surfaces: Prediction of Co and Ni as Effective Dopants for Electrocatalysis. *J. Am. Chem. Soc.* **2012**, *134*, 13296–13309.

(72) Sheng, T.; Lin, W.-F.; Hardacre, C.; Hu, P. Role of Water and Adsorbed Hydroxyls on Ethanol Electrochemistry on Pd: New Mechanism, Active Centers, and Energetics for Direct Ethanol Fuel Cell Running in Alkaline Medium. *J. Phys. Chem. C* **2014**, *118*, 5762–5772.

(73) Maier, S.; Salmeron, M. How Does Water Wet a Surface? *Acc. Chem. Res.* **2015**, *48*, 2783–2790.

(74) Stoerzinger, K. A.; Hong, W. T.; Azimi, G.; Giordano, L.; Lee, Y.-L.; Crumlin, E. J.; Biegalski, M. D.; Bluhm, H.; Varanasi, K. K.; Shao-Horn, Y. Reactivity of Perovskites with Water: Role of Hydroxylation in Wetting and Implications for Oxygen Electrocatalysis. *J. Phys. Chem. C* **2015**, *119*, 18504–18512.

(75) Carchini, G.; García-Melchor, M.; Łodziana, Z.; López, N. Understanding and Tuning the Intrinsic Hydrophobicity of Rare-Earth Oxides: A DFT+U Study. *ACS Appl. Mater. Interfaces* **2016**, *8*, 152–160.

(76) Rana, A. et al. Correlation of nanoscale behaviour of forces and macroscale surface wettability. *Nanoscale* **2016**, *8*, 15597–15603.

(77) Wang, S.; Wang, T.; Ge, P.; Xue, P.; Ye, S.; Chen, H.; Li, Z.; Zhang, J.; Yang, B. Controlling Flow Behavior of Water in Microfluidics with a Chemically Patterned Anisotropic Wetting Surface. *Langmuir* **2015**, *31*, 4032–4039.

(78) Mu, R.; Zhao, Z.-j.; Dohnálek, Z.; Gong, J. Structural motifs of water on metal oxide surfaces. *Chem. Soc. Rev.* **2017**, *46*, 1785–1806.

(79) Kharche, N.; Muckerman, J. T.; Hybertsen, M. S. First-Principles Approach to Calculating Energy Level Alignment at Aqueous Semiconductor Interfaces. *Phys. Rev. Lett.* **2014**, *113*, 176802.

(80) Ma, S.-Y.; Liu, L.-M.; Wang, S.-Q. Water Film Adsorbed on the α-Al2O3(0001) Surface: Structural Properties and Dynamical Behaviors from First-Principles Molecular Dynamics Simulations. *J. Phys. Chem. C* **2016**, *120*, 5398–5409.

(81) Kharche, N.; Hybertsen, M. S.; Muckerman, J. T. Computational investigation of structural and electronic properties of aqueous interfaces of GaN, ZnO, and a GaN/ZnO alloy. *Phys. Chem. Chem. Phys.* **2014**, *16*, 12057–12066.

(82) Farnesi Camellone, M.; Negreiros Ribeiro, F.; Szabová, L.; Tateyama, Y.; Fabris, S. Catalytic Proton Dynamics at the Water/Solid Interface of Ceria-Supported Pt Clusters. *J. Am. Chem. Soc.* **2016**, *138*, 11560–11567.

(83) Boily, J.-F.; Yeşilbaş, M.; Md. Musleh Uddin, M.; Baiqing, L.; Trushkina, Y.; Salazar-Alvarez, G. Thin Water Films at Multifaceted Hematite Particle Surfaces. *Langmuir* **2015**, *31*, 13127–13137.

(84) Mirabella Francesca,; Zaki Eman,; Ivars-Barceló Francisco,; Li Xiaoke,; Paier Joachim,; Sauer Joachim,; Shaikhutdinov Shamil,; Freund Hans-Joachim, Cooperative Formation of Long-Range Ordering in Water Ad-layers on Fe3O4(111) Surfaces. *Angew. Chem., Int. Ed.* **2017**, *57*, 1409–1413.

(85) Wang, Z.-T.; Wang, Y.-G.; Mu, R.; Yoon, Y.; Dahal, A.; Schenter, G. K.; Glezakou, V.-A.; Rousseau, R.; Lyubinetsky, I.; Dohnálek, Z. Probing equilibrium of molecular and deprotonated water on TiO2(110). *PNAS* **2017**, 201613756.

(86) Ossowski, T.; Da Silva, J. L. F.; Kiejna, A. Water adsorption on the stoichiometric and defected Fe(110) surfaces. *Surf. Sci.* **2018**, *668*, 144–149.

(87) Han, C.; Zhang, C.; Liu, X.; Huang, H.; Zhuang, S.; Han, P.; Wu, X. Effects of alloying on oxidation and dissolution corrosion of the surface of γ-Fe(111): a DFT study. *J. Mol. Model.* **2015**, *21*, 181.

(88) Raschke, T. M. Water structure and interactions with protein surfaces. *Current Opinion in Structural Biology* **2006**, *16*, 152–159.

(89) Ball, P. Water as an Active Constituent in Cell Biology. *Chem. Rev.* **2008**, *108*, 74–108.

(90) Vojvodic, A.; Norskov, J. K.; Abild-Pedersen, F. Electronic Structure Effects in Transition Metal Surface Chemistry. *Top. Catal.* **2014**, *57*, 25–32.

(91) Michaelides, A.; Ranea, V. A.; de Andres, P. L.; King, D. A. General Model for Water Monomer Adsorption on Close-Packed Transition and Noble Metal Surfaces. *Phys. Rev. Lett.* **2003**, *90*, 216102.

(92) Kiejna, A.; Ossowski, T. *Reference Module in Chemistry, Molecular Sciences and Chemical Engineering*; Elsevier, 2017.

(93) Tereshchuk, P.; Da Silva, J. L. F. Ethanol and Water Adsorption on Close-Packed 3d, 4d, and 5d Transition-Metal Surfaces: A Density Functional Theory Investigation with van der Waals Correction. *J. Phys. Chem. C* **2012**, *116*, 24695–24705.

(94) Cabral do Couto, P.; Estacio, S. G.; Costa Cabral, B. J. The Kohn-Sham density of states and band gap of water: From small clusters to liquid water. *J. Chem. Phys.* **2005**, *123*, 054510.

(95) Ning, C. G.; Hajgato, B.; Huang, Y. R.; Zhang, S. F.; Liu, K.; Luo, Z. H.; Knippenberg, S.; Deng, J. K.; Deleuze, M. S. High resolution electron momentum spectroscopy of the valence orbitals of water. *Chem. Phys.* **2008**, *343*, 19–30.

(96) Laasonen, K.; Sprik, M.; Parrinello, M.; Car, R. ''Ab initio'' liquid water. *J. Chem. Phys.* **1993**, *99*, 9080–9089.

(97) Satoh, S.; Fujimoto, H.; Kobayashi, H. Theoretical Study of NH3 Adsorption on Fe(110) and Fe(111) Surfaces. *J. Phys. Chem. B* **2006**, *110*, 4846–4852.

(98) Wang, C.-C.; Siao, S. S.; Jiang, J.-C. Density Functional Theory Study of NHx (x = 0-3) and N2 Adsorption on IrO2(110) Surfaces. *J. Phys. Chem. C* **2010**, *114*, 18588–18593.

(99) Beheshtian, J.; Peyghan, A. A.; Bagheri, Z. Ab initio study of NH3 and H2O adsorption on pristine and Na-doped MgO nanotubes. *Struct. Chem.* **2013**, *24*, 165–170.

(100) Norskov, J. K.; Studt, F.; Abild-Pedersen, F.; Bligaard, T. *Fundamental Concepts in Heterogeneous Catalysis*; John Wiley & Sons, Inc, 2014; pp 114–137.

(101) Garrity, K.; Kakekhani, A.; Kolpak, A.; Ismail-Beigi, S. Ferroelectric surface chemistry: First-principles study of the PbTiO3 surface. *Phys. Rev. B* **2013**, *88*, 045401.

(102) Kakekhani, A.; Ismail-Beigi, S. Polarization-driven catalysis via ferroelectric oxide surfaces. *Phys. Chem. Chem. Phys.* **2016**, *18*, 19676–19695.

(103) Christian, M. S.; Otero-de-la Roza, A.; Johnson, E. R. Surface Adsorption from the Exchange-Hole Dipole Moment Dispersion Model. *J. Chem. Theory Comput.* **2016**, *12*, 3305–3315.

(104) Zhu, S.-B.; Philpott, M. R. Interaction of water with metal surfaces. *J. Chem. Phys.* **1994**, *100*, 6961–6968.

(105) Bilic, A.; Reimers, J. R.; Hush, N. S.; Hafner, J. Adsorption of ammonia on the gold (111) surface. *J. Chem. Phys.* **2002**, *116*, 8981–8987.

(106) Bagus, P. S.; Hermann, K.; Bauschlicher, C. W. On the nature of the bonding of lone pair ligands to a transition metal. *J. Chem. Phys.* **1984**, *81*, 1966–1974.

(107) Carrasco, J.; Klimes, J.; Michaelides, A. The role of van der Waals forces in water adsorption on metals. *J. Chem. Phys.* **2013**, *138*, 024708.

(108) Hamada, I.; Lee, K.; Morikawa, Y. Interaction of water with a metal surface: Importance of van der Waals forces. *Phys. Rev. B* **2010**, *81*, 115452.

(109) Xue, Y. Water monomer interaction with gold nanoclusters from van der Waals density functional theory. *J. Chem. Phys.* **2012**, *136*, 024702.

(110) Liang Hu, X.; Carrasco, J.; Klimes, J.; Michaelides, A. Trends in water monomer adsorption and dissociation on flat insulating surfaces. *Phys. Chem. Chem. Phys.* **2011**, *13*, 12447–12453.

(111) Fernandez-Torre, D.; Kosmider, K.; Carrasco, J.; Ganduglia-Pirovano, M. V.; Perez, R. Insight into the Adsorption of Water on the Clean CeO2(111) Surface with van der Waals and Hybrid Density Functionals. *J. Phys. Chem. C* **2012**, *116*, 13584–13593.

(112) Kebede, G. G.; Spangberg, D.; Mitev, P. D.; Broqvist, P.; Hermansson, K. Comparing van der Waals DFT methods for water on NaCl(001) and MgO(001). *J. Chem. Phys.* **2017**, *146*, 064703.

(113) Bligaard, T.; Norskov, J. K. *Chemical Bonding at Surfaces and Interfaces*; Elsevier: Amsterdam, 2008; pp 255–321.

(114) Norskov, J. K.; Abild-Pedersen, F.; Studt, F.; Bligaard, T. Density functional theory in surface chemistry and catalysis. *PNAS* **2011**, *108*, 937–943.

(115) Acerbi, N.; Tsang, S. C. E.; Jones, G.; Golunski, S.; Collier, P. Rationalization of Interactions in Precious Metal/Ceria Catalysts Using the d-Band Center Model. *Angew. Chem. Int. Ed.* **2013**, *52*, 7737–7741.

(116) Calle-Vallejo, F.; Koper, M. T. M. First-principles computational electrochemistry: Achievements and challenges. *Electrochim. Acta* **2012**, *84*, 3–11.

(117) Henkelman, G.; Arnaldsson, A.; Jonsson, H. A fast and robust algorithm for Bader decomposition of charge density. *Comput. Mater. Sci.* **2006**, *36*, 354–360.

(118) Sanville, E.; Kenny, S. D.; Smith, R.; Henkelman, G. Improved grid-based algorithm for Bader charge allocation. *J. Comput. Chem.* **2007**, *28*, 899–908.

(119) Kolaczkiewicz, J.; Bauer, E. The dipole moments of noble and transition metal atoms adsorbed on W(110) and W(211) surfaces. *Surf. Sci.* **1985**, *160*, 1–11.

(120) Miedema, A. R. The electronegativity parameter for transition metals: Heat of formation and charge transfer in alloys. *J. Less-Common Met.* **1973**, *32*, 117–136.

(121) Vilella, L.; Studt, F. The Stability of Copper Oxo Species in Zeolite Frameworks. *Eur. J. Inorg. Chem.* **2016**, *2016*, 1514–1520.

(122) Tomkins, P.; Mansouri, A.; Bozbag, S. E.; Krumeich, F.; Park, M. B.; Alayon, E. M. C.; Ranocchiari, M.; van Bokhoven, J. A. Isothermal Cyclic Conversion of Methane into Methanol over Copper-Exchanged Zeolite at Low Temperature. *Angew. Chem.* **2016**, *128*, 5557–5561.

(123) Kakekhani, A.; Ismail-Beigi, S. Ferroelectric-Based Catalysis: Switchable Surface Chemistry. *ACS Catal.* **2015**, *5*, 4537–4545.

(124) Coulson, C. A.; Maccoll, A.; Sutton, L. E. The polarizability of molecules in strong electric fields. *Trans. Faraday Soc.* **1952**, *48*, 106–113.

(125) Brauman, J. I.; Blair, L. K. Gas-phase acidities of alcohols. *J. Am. Chem. Soc.* **1970**, *92*, 5986–5992.

(126) Wang, C.-C.; Yang, Y.-J.; Jiang, J.-C. DFT Study of NHx (x = 1-3) Adsorption on RuO2(110) Surfaces. *J. Phys. Chem. C* **2009**, *113*, 2816–2821.

(127) Calzolari, A.; Catellani, A. Water Adsorption on Nonpolar ZnO(1010) Surface: A Microscopic Understanding. *J. Phys. Chem. C* **2009**, *113*, 2896–2902.

(128) Kaewmaraya, T.; Pathak, B.; Araujo, C. M.; Rosa, A. L.; Ahuja, R. Water adsorption on ZnO(1010): The role of intrinsic defects. *EPL* **2012**, *97*, 17014.

(129) Raymand, D.; van Duin, A. C. T.; Spangberg, D.; Goddard, W. A.; Hermansson, K. Water adsorption on stepped ZnO surfaces from MD simulation. *Surf. Sci.* **2010**, *604*, 741–752.

(130) Gillan, M. J.; Alfe, D.; Michaelides, A. Perspective: How good is DFT for water? *J. Chem. Phys.* **2016**, *144*, 130901.

(131) Ming, Y.; Kumar, N.; Siegel, D. J. Water Adsorption and Insertion in MOF-5. *ACS Omega* **2017**, *2*, 4921–4928.

(132) Hammer, B.; Norskov, J. K. *Advances in Catalysis*; Impact of Surface Science on Catalysis; Academic Press, 2000; Vol. 45; pp 71–129.

(133) Medford, A. J.; Wellendorff, J.; Vojvodic, A.; Studt, F.; Abild-Pedersen, F.; Jacobsen, K. W.; Bligaard, T.; Norskov, J. K. Assessing the reliability of calculated catalytic ammonia synthesis rates. *Science* **2014**, *345*, 197–200.

(134) Shannon, R. D. Revised effective ionic radii and systematic studies of interatomic distances in halides and chalcogenides. *Acta Crystallogr., Sect. A: Cryst. Phys., Diffr., Theor. Gen. Crystallogr.* **1976**, *32*, 751–767.

(135) Hass, K. C.; Schneider, W. F.; Curioni, A.; Andreoni, W. The Chemistry of Water on Alumina Surfaces: Reaction Dynamics from First Principles. *Science* **1998**, *282*, 265–268.

(136) Ahn, J.; Rabalais, J. W. Composition and structure of the Al2O3{0001}-(1*1) surface. *Surf. Sci.* **1997**, *388*, 121–131.

(137) Ranea, V. A.; Schneider, W. F.; Carmichael, I. DFT characterization of coverage

dependent molecular water adsorption modes on α-Al2O3(0001). *Surf. Sci.* **2008**, *602*, 268–275.

(138) Guenard, P.; Renaud, G.; Barbier, A.; Gautier-Soyer, M. Determination of the α-Al2O3(0001) Surface Relaxation and Termination by Measurements of Crystal Truncation Rods. *Surf. Rev. Lett.* **1998**, *05*, 321–324.

(139) Meyer, B.; Woll, C.; Silber, D.; Bebensee, F.; Traeger, F.; Buchholz, M.; Kowalski, P. M. Adsorbate-induced lifting of substrate relaxation is a general mechanism governing titania surface chemistry. *Nat. Commun.* **2016**, *7*, 12888.

(140) Grimme, S. Semiempirical GGA-type density functional constructed with a long-range dispersion correction. *J. Comput. Chem.* **2006**, *27*, 1787–1799.

(141) Wagner, C.; Fournier, N.; Ruiz, V. G.; Li, C.; Mullen, K.; Rohlfing, M.; Tkatchenko, A.; Temirov, R.; Tautz, F. S. Non-additivity of molecule-surface van der Waals potentials from force measurements. *Nat. Commun.* **2014**, *5*.

(142) Ruiz, V. G.; Liu, W.; Zojer, E.; Scheffler, M.; Tkatchenko, A. Density-Functional Theory with Screened van der Waals Interactions for the Modeling of Hybrid Inorganic-Organic Systems. *Phys. Rev. Lett.* **2012**, *108*, 146103.

(143) Tkatchenko, A.; Scheffler, M. Accurate Molecular Van Der Waals Interactions from Ground-State Electron Density and Free-Atom Reference Data. *Phys. Rev. Lett.* **2009**, *102*, 073005.

(144) Jin, W.; Chen, G.; Duan, X.; Yin, Y.; Ye, H.; Wang, D.; Yu, J.; Mei, X.; Wu, Y. Adsorption behavior of formaldehyde on ZnO (1010) surface: A first principles study. *Appl. Surf. Sci.* **2017**, *423*, 451–456.

(145) Andersson, K.; Nikitin, A.; Pettersson, L. G. M.; Nilsson, A.; Ogasawara, H. Water Dissociation on Ru(001): An Activated Process. *Phys. Rev. Lett.* **2004**, *93*, 196101.

(146) Halwidl, D.; Stöger, B.; Mayr-Schmölzer, W.; Pavelec, J.; Fobes, D.; Peng, J.; Mao, Z.; Parkinson, G. S.; Schmid, M.; Mittendorfer, F.; Redinger, J.; Diebold, U. Adsorption of water at the SrO surface of ruthenates. *Nat. Mater.* **2016**, *15*, 450–455.

(147) Ranea, V. A.; Carmichael, I.; Schneider, W. F. DFT Investigation of Intermediate Steps in the Hydrolysis of α-Al2O3(0001). *J. Phys. Chem. C* **2009**, *113*, 2149–2158.

(148) Batzill, M.; Bergermayer, W.; Tanaka, I.; Diebold, U. Tuning the chemical functionality of a gas sensitive material: Water adsorption on SnO2(101). *Surf. Sci.* **2006**, *600*, 29–32.

(149) Santarossa, G.; Hahn, K.; Baiker, A. Free Energy and Electronic Properties of Water Adsorption on the SnO2(110) Surface. *Langmuir* **2013**, *29*, 5487–5499.

(150) Zhou, X.; Hensen, E. J. M.; van Santen, R. A.; Li, C. DFT Simulations of Water Adsorption and Activation on Low-Index α-Ga2O3 Surfaces. *Chem. Eur. J.* **2014**, *20*, 6915–6926.

(151) Phatak, A. A.; Delgass, W. N.; Ribeiro, F. H.; Schneider, W. F. Density Functional Theory Comparison of Water Dissociation Steps on Cu, Au, Ni, Pd, and Pt. *J. Phys. Chem. C* **2009**, *113*, 7269–7276.

(152) Kiawi, D. M.; Chernyy, V.; Oomens, J.; Buma, W. J.; Jamshidi, Z.; Visscher, L.; Waters, L. B. F. M.; Bakker, J. M. Water Dissociation upon Adsorption onto Free Iron Clusters Is Size Dependent. *J. Phys. Chem. Lett.* **2016**, *7*, 2381–2387.

(153) Thissen, P.; Grundmeier, G.; Wippermann, S.; Schmidt, W. G. Water adsorption on the alpha-Al2O3(0001) surface. *Phys. Rev. B* **2009**, *80*, 245403.

(154) Lu, Y.-H.; Wu, S.-Y.; Chen, H.-T. H2O Adsorption/Dissociation and H2 Generation by the Reaction of H2O with Al2O3 Materials: A First-Principles Investigation. *J. Phys. Chem. C* **2016**, *120*, 21561–21570.

(155) Heiden, S.; Yue, Y.; Kirsch, H.; Wirth, J.; Saalfrank, P.; Campen, R. K. Water Dissociative Adsorption on α-Al2O3(1120) Is Controlled by Surface Site Undercoordination, Density, and Topology. *J. Phys. Chem. C* **2018**, *122*, 6573–6584.

(156) Kirsch, H.; Wirth, J.; Tong, Y.; Wolf, M.; Saalfrank, P.; Campen, R. K. Experimental Characterization of Unimolecular Water Dissociative Adsorption on α-Alumina. *J. Phys. Chem. C* **2014**, *118*, 13623–13630.

(157) Carrasco, J.; Illas, F.; Lopez, N. Dynamic Ion Pairs in the Adsorption of Isolated Water Molecules on Alkaline-Earth Oxide (001) Surfaces. *Phys. Rev. Lett.* **2008**, *100*, 016101.

(158) Guhl, H.; Miller, W.; Reuter, K. Water adsorption and dissociation on SrTiO3(001) revisited: A density functional theory study. *Phys. Rev. B* **2010**, *81*, 155455.

(159) Castelli, I. E.; Man, I.-C.; Soriga, S.-G.; Parvulescu, V.; Halck, N. B.; Rossmeisl, J. Role of the Band Gap for the Interaction Energy of Coadsorbed Fragments. *J. Phys. Chem. C* **2017**, *121*, 18608–18614.

(160) Chretien, S.; Metiu, H. Acid–Base Interaction and Its Role in Alkane Dissociative Chemisorption on Oxide Surfaces. *J. Phys. Chem. C* **2014**, *118*, 27336–27342.

(161) Yoshida, Y.; Nagai, I.; Ikeda, S.-I.; Shirakawa, N.; Kosaka, M.; Môri, N. Quasi-two-dimensional metallic ground state of Ca3Ru2O7. *Phys. Rev. B* **2004**, *69*, 220411.

(162) Halwidl, D.; Mayr-Schmölzer, W.; Fobes, D.; Peng, J.; Mao, Z.; Schmid, M.; Mittendorfer, F.; Redinger, J.; Diebold, U. Ordered hydroxyls on Ca 3 Ru 2 O 7 (001). *Nat. Commun.* **2017**, *8*, 23.

(163) Jung, J.; Shin, H.-J.; Kim, Y.; Kawai, M. Activation of Ultrathin Oxide Films for Chemical Reaction by Interface Defects. *J. Am. Chem. Soc.* **2011**, *133*, 6142–6145.

(164) Jung, J.; Shin, H.-J.; Kim, Y.; Kawai, M. Controlling water dissociation on an ultrathin MgO film by tuning film thickness. *Phys. Rev. B* **2010**, *82*, 085413.

(165) Honkala, K.; Hellman, A.; Grönbeck, H. Water Dissociation on MgO/Ag(100): Support Induced Stabilization or Electron Pairing? *J. Phys. Chem. C* **2010**, *114*, 7070–7075.

(166) Kakekhani, A.; Ismail-Beigi, S. Ferroelectric oxide surface chemistry: water splitting via pyroelectricity. *J. Mater. Chem. A* **2016**, *4*, 5235–5246.

(167) Stair, P. C. The concept of Lewis acids and bases applied to surfaces. *J. Am. Chem. Soc.* **1982**, *104*, 4044–4052.

(168) Klopman, G. Chemical reactivity and the concept of charge- and frontier-controlled reactions. *J. Am. Chem. Soc.* **1968**, *90*, 223–234.

(169) Jensen, W. B. *The Lewis acid-base concepts : an overview / William B. Jensen*; Wiley: New York, p. 342-343.

(170) Lessio, M.; Dieterich, J. M.; Carter, E. A. Hydride Transfer at the GaP(110)/Solution Interface: Mechanistic Implications for CO2 Reduction Catalyzed by Pyridine. *J. Phys. Chem. C* **2017**, *121*, 17321–17331.

(171) M. Ugeda, M.; Bradley, A. J.; Rodrigo, L.; Yu, M.; Liu, W.; Doak, P.; Riss, A.; Neaton, J. B.; Tilley, T. D.; Perez, R.; Crommie, M. F. Covalent Functionalization of GaP(110) Surfaces via a Staudinger-Type Reaction with Perfluorophenyl Azide. *J. Phys. Chem. C* **2016**, *120*, 26448–26452.

(172) Kronawitter, C. X.; Lessio, M.; Zhao, P.; Riplinger, C.; Boscoboinik, A.; Starr, D. E.; Sutter, P.; Carter, E. A.; Koel, B. E. Observation of Surface-Bound Negatively Charged Hydride and Hydroxide on GaP(110) in H2O Environments. *J. Phys. Chem. C* **2015**, *119*, 17762–17772.

(173) Jeon, S.; Kim, H.; Goddard, W. A.; Atwater, H. A. DFT Study of Water Adsorption and Decomposition on a Ga-Rich GaP(001)(2*4) Surface. *J. Phys. Chem. C* **2012**, *116*, 17604–17612.

(174) Wood, B. C.; Schwegler, E.; Choi, W. I.; Ogitsu, T. Surface Chemistry of GaP(001) and InP(001) in Contact with Water. *J. Phys. Chem. C* **2014**, *118*, 1062–1070.

(175) Riplinger, C.; Carter, E. A. Cooperative Effects in Water Binding to Cuprous Oxide Surfaces. *J. Phys. Chem. C* **2015**, *119*, 9311–9323.

(176) Kanan, D. K.; Keith, J. A.; Carter, E. A. Water adsorption on MnO:ZnO(001) — From single molecules to bilayer coverage. *Surf. Sci.* **2013**, *617*, 218–224.

(177) Kanan, D. K.; Keith, J. A.; Carter, E. A. First-Principles Modeling of Electrochemical Water Oxidation on MnO:ZnO(001). *ChemElectroChem* **2014**, *1*, 407–415.

(178) Patrick, C. E.; Giustino, F. Structure of a Water Monolayer on the Anatase TiO2(101) Surface. *Phys. Rev. Applied* **2014**, *2*, 014001.

(179) Sun, C.; Liu, L.-M.; Selloni, A.; Qing (Max) Lu, G.; C. Smith, S. Titania - water interactions: a review of theoretical studies. *Journal of Materials Chemistry* **2010**, *20*, 10319–10334.

(180) Meier, M.; Hulva, J.; Jakub, Z.; Pavelec, J.; Setvin, M.; Bliem, R.; Schmid, M.; Diebold, U.; Franchini, C.; Parkinson, G. S. Water Agglomerates on Fe3O4(001). *arXiv:1801.09601 [physics]* **2018**, arXiv: 1801.09601.

(181) Agosta, L.; Zollo, G.; Arcangeli, C.; Buonocore, F.; Gala, F.; Celino, M. Water driven adsorption of amino acids on the (101) anatase TiO 2 surface: an ab initio study. *Phys. Chem. Chem. Phys.* **2015**, *17*, 1556–1561.

(182) Kempisty, P.; Strak, P.; Sakowski, K.; Krukowski, S. DFT study of ammonia desorption from the GaN(0001) surface covered with a NH3/NH2 mixture. *J. Cryst. Growth* **2014**, *403*, 105–109.

(183) Zhang, J.-S.; Liu, H.-C.; Shi, F.; Yu, F.; Liu, Y.; Xiao, C.; Lan, Q. Adsorption and dissociation of H2O on the Ga-rich GaAs(001)-(42) surface: DFT and DFT-D computations with a Ga7As8H11 cluster model. *Comput. Theor. Chem.* **2015**, *1064*, 51–55.

(184) Triggiani, L.; Muñoz-García, A. B.; Agostiano, A.; Pavone, M. First-principles study of trimethylamine adsorption on anatase TiO2 nanorod surfaces. *Theor. Chem. Acc.* **2015**, *134*, 119.

(185) Dahal, A.; Dohnálek, Z. Formation of Metastable Water Chains on Anatase TiO2(101). *J. Phys. Chem. C* **2017**, *121*, 20413–20418.

(186) Kim, D. H.; Bae, S.-S.; Hong, S.; Kim, S. Atomic and electronic structure of methanol on Ge(100). *Surf. Sci.* **2010**, *604*, 129–135.

(187) Wang, X.; Xu, X. Mechanisms for NH3 Decomposition on the Si(111)-7 7 Surface: A DFT Cluster Model Study. *J. Phys. Chem. C* **2007**, *111*, 16974–16981.

(188) He, Y.; Tilocca, A.; Dulub, O.; Selloni, A.; Diebold, U. Local ordering and electronic signatures of submonolayer water on anatase TiO2(101). *Nat. Mater.* **2009**, *8*, 585–589.

(189) Jung,; Lee, J. Y.; Hong, S.; Kim, S. Study of Adsorption and Decomposition of H2O on Ge(100). *J. Phys. Chem. B* **2005**, *109*, 24445–24449.

(190) M. Montemore, M.; Will Medlin, J. Scaling relations between adsorption energies for computational screening and design of catalysts. *Catal. Sci. Technol.* **2014**, *4*, 3748–3761.

(191) Calle-Vallejo, F.; Martínez, J. I.; García-Lastra, J. M.; Rossmeisl, J.; Koper, M. T. M. Physical and Chemical Nature of the Scaling Relations between Adsorption Energies of Atoms on Metal Surfaces. *Phys. Rev. Lett.* **2012**, *108*, 116103.

(192) Norskov, J. K.; Bligaard, T.; Rossmeisl, J.; Christensen, C. H. Towards the computational design of solid catalysts. *Nat. Chem.* **2009**, *1*, nchem.121.

(193) T. Hong, W.; Risch, M.; A. Stoerzinger, K.; Grimaud, A.; Suntivich, J.; Shao-Horn, Y. Toward the rational design of non-precious transition metal oxides for oxygen electrocatalysis. *Energy Environ. Sci.* **2015**, *8*, 1404–1427.

(194) Li, Z.; Ma, X.; Xin, H. Feature engineering of machine-learning chemisorption models for catalyst design. *Catal. Today* **2017**, *280*, 232–238.

(195) Seh, Z. W.; Kibsgaard, J.; Dickens, C. F.; Chorkendorff, I.; Nørskov, J. K.; Jaramillo, T. F. Combining theory and experiment in electrocatalysis: Insights into materials design. *Science* **2017**, *355*, eaad4998.

(196) Montoya, J. H.; Seitz, L. C.; Chakthranont, P.; Vojvodic, A.; Jaramillo, T. F.; Nørskov, J. K. Materials for solar fuels and chemicals. *Nat. Mater.* **2017**, *16*, 70.

(197) Kohn, W.; Sham, L. J. Self-Consistent Equations Including Exchange and Correlation Effects. *Phys. Rev.* **1965**, *140*, A1133–A1138.

(198) Hohenberg, P.; Kohn, W. Inhomogeneous Electron Gas. *Phys. Rev.* **1964**, *136*, B864–B871.

(199) Giannozzi, P. et al. QUANTUM ESPRESSO: a modular and open-source software project for quantum simulations of materials. *J. Phys.: Condens. Matter* **2009**, *21*, 395502.

Figure 13: For Table of Contents only

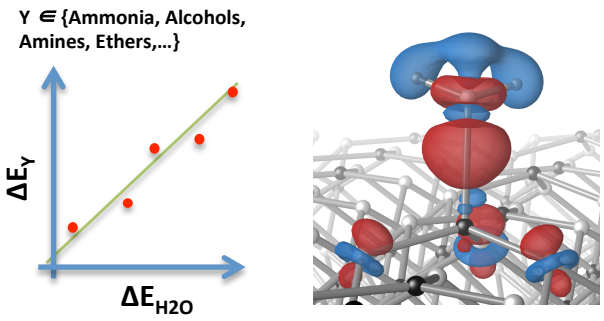

Synopsis (For Table of Contents Only)

Correlations between binding energies of a class of closed-shell molecules (e.g., water, ammonia, alcohols) are shown and the main bonding mechanisms are identified.